AD-A042 177 NAVAL POSTGRADUATE SCHOOL MONTEREY CALIF F/G 4/2
THE RELATIONSHIP BETWEEN FNWC SURFACE WIND ANALYSIS AND NOAA/NE--ETC(U)
JUN 77 G H BERRY

UNCLASSIFIED NL

| OF |
AD A042177

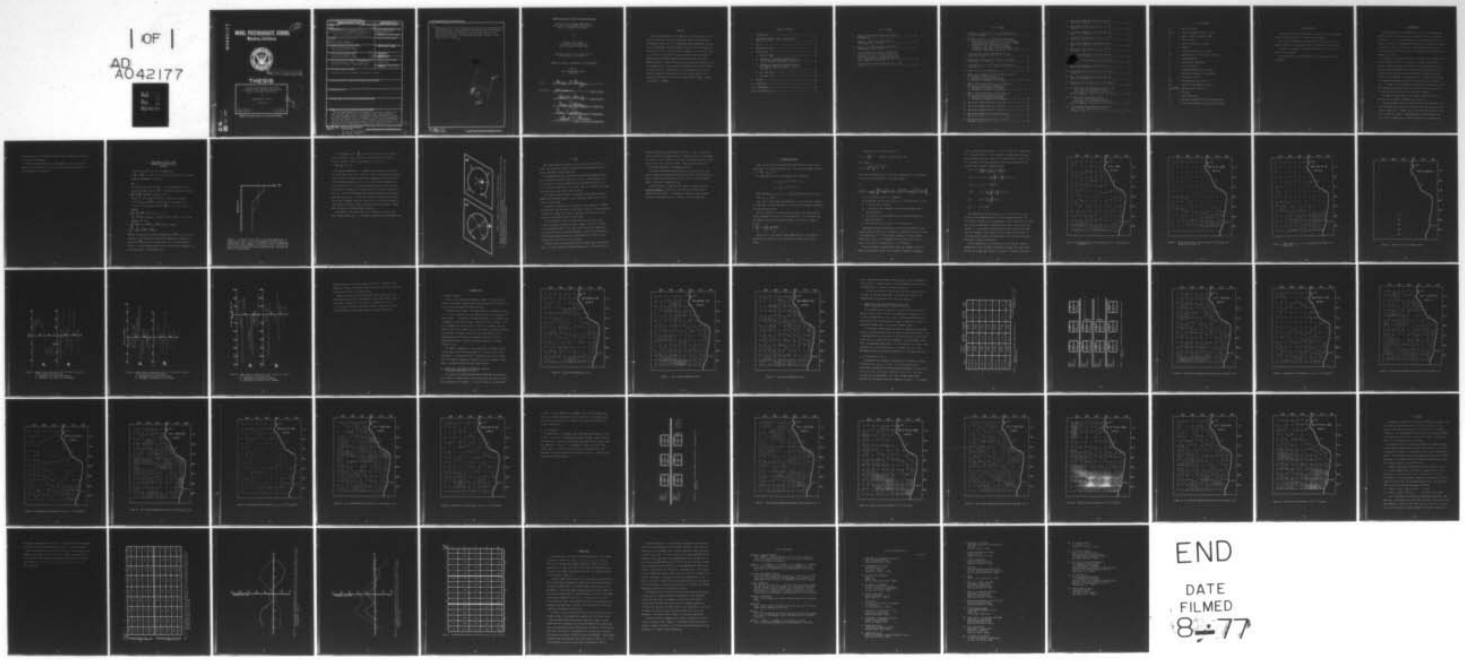

END

DATE FILMED
8-77

NAVAL POSTGRADUATE SCHOOL
Monterey, California

THESIS

THE RELATIONSHIP BETWEEN FNWC SURFACE
WIND ANALYSIS AND NOAA/NESS GOSSTCOMP (SST)
DATA IN THE EASTERN SOUTH PACIFIC

by

George Hamilton Berry

June 1977

Thesis Advisor: R. L. Haney
Thesis Advisor: J. B. Wickham

Approved for public release; distribution unlimited.

SECURITY CLASSIFICATION OF THIS PAGE (When Data Entered)

REPORT DOCUMENTATION PAGE		READ INSTRUCTIONS BEFORE COMPLETING FORM
1. REPORT NUMBER (6)	2. GOVT ACCESSION NO.	3. RECIPIENT'S CATALOG NUMBER (9)
4. TITLE (and Subtitle) The Relationship between FNWC Surface Wind Analysis and NOAA/NESS GOSSTCOMP (SST) Data in the Eastern South Pacific.		5. TYPE OF REPORT & PERIOD COVERED Master's Thesis; June 1977
		6. PERFORMING ORG. REPORT NUMBER
7. AUTHOR(s) (10) George Hamilton Berry		8. CONTRACT OR GRANT NUMBER(s)
9. PERFORMING ORGANIZATION NAME AND ADDRESS Naval Postgraduate School Monterey, California 93940		10. PROGRAM ELEMENT, PROJECT, TASK AREA & WORK UNIT NUMBERS
11. CONTROLLING OFFICE NAME AND ADDRESS Naval Postgraduate School Monterey, California 93940 (11)		12. REPORT DATE June 1977
		13. NUMBER OF PAGES 65
14. MONITORING AGENCY NAME & ADDRESS(if different from Controlling Office) Naval Postgraduate School Monterey, California 93940 (12) 62p.		15. SECURITY CLASS. (of this report) Unclassified
		15a. DECLASSIFICATION/DOWNGRADING SCHEDULE

16. DISTRIBUTION STATEMENT (of this Report)

Approved for public release; distribution unlimited.

17. DISTRIBUTION STATEMENT (of the abstract entered in Block 20, if different from Report)

18. SUPPLEMENTARY NOTES

19. KEY WORDS (Continue on reverse side if necessary and identify by block number)

20. ABSTRACT (Continue on reverse side if necessary and identify by block number)

Sea surface temperature (SST) anomalies on the daily synoptic time scale from National Oceanic and Atmospheric Administration/National Environmental Satellite Service (NOAA/NESS) Global Operational SST Computationa (GOSSTCOMP) data in the Eastern South Pacific are compared to deviations of similar time scale from the means of both the wind stress curl and the friction velocity cubed as derived from Fleet Numerical Weather Central's (FNWC) mercator global band surface wind field.

Next Page

DD FORM 1 JAN 73 1473 (Page 1) EDITION OF 1 NOV 65 IS OBSOLETE S/N 0102-014-6601

Example patterns of those variables as well as mean and unaltered fields are presented here. High correlations between the sea surface temperature deviations and the deviations of wind stress curl and friction velocity cubed were not attained at any log, owing largely to the paucity and poor quality of surface wind and satellite data. Further investigation is needed.

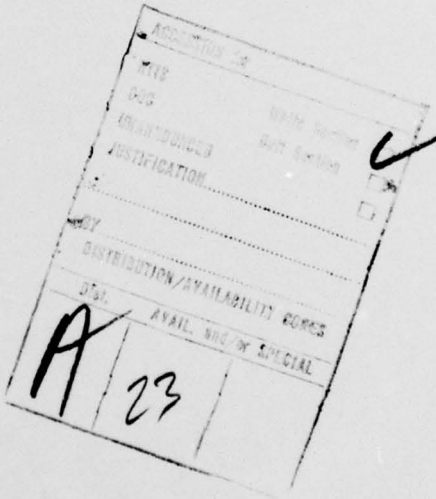

Approved for public release; distribution unlimited

The Relationship between FNWC Surface Wind Analysis and NOAA/NESS GOSSTCOMP (SST) Data in the Eastern South Pacific

by

George Hamilton Berry
Lieutenant, United States Navy
B.S., University of Utah, 1972

Submitted in partial fulfillment of the
requirements for the degree of

MASTER OF SCIENCE IN METEOROLOGY AND OCEANOGRAPHY

from the

NAVAL POSTGRADUATE SCHOOL
June 1977

Author George H. Berry

Approved by: J B Wickham
Thesis Advisor

Robert L. Haney
Thesis Advisor

George J. Haltiner
Chairman, Department of Meteorology

Dale F. Leipper
Chairman, Department of Oceanography

Robert R. Brown
Dean of Science and Engineering

ABSTRACT

Sea surface temperature (SST) anomalies on the daily synoptic time scale from National Oceanic and Atmospheric Administration/National Environmental Satellite Service (NOAA/NESS) Global Operational SST Computation (GOSSTCOMP) data in the Eastern South Pacific are compared to deviations of similar time scale from the means of both the wind stress curl and the friction velocity cubed as derived from Fleet Numerical Weather Central's (FNWC) mercator global band surface wind field. Example patterns of those variables as well as mean and unaltered fields are presented here. High correlations between the sea surface temperature deviations and the deviations of wind stress curl and friction velocity cubed were not attained at any log, owing largely to the paucity and poor quality of surface wind and satellite data. Further investigation is needed.

TABLE OF CONTENTS

LIST OF TABLES

LIST OF FIGURES

LIST OF SYMBOLS

C_d	=	drag coefficient
$curl_z\ \tau$	=	vertical component of the curl of Tau
C_v	=	specific heat at constant volume
f	=	coriolis factor
$\dot{H}$	=	rate of heating per unit mass
P	=	pressure
$\dot{Q}$	=	rate of heating per unit volume
$R(z)$	=	absorption of solar radiation in the sea
T	=	ocean temperature
T_s	=	surface ocean temperature
U_*	=	friction velocity
U	=	west-east component of wind vector
v	=	south-north component of wind vector
$\vec{V}$	=	surface wind vector
$\overline{W_e}$	=	mean Ekman vertical velocity
ρ_{wo}	=	density of ocean water at surface
$\rho_{wo}C_v(\overline{W'T'})$	=	upward turbulent heat flux
ϕ	=	latitude
$\vec{\tau}$	=	wind stress vector
τ_x	=	west-east component of the wind stress vector
τ_y	=	south-north component of the wind stress vector

ACKNOWLEDGMENTS

The author wishes to thank DMA-IAGS, Canal Zone, for the encouragement to study the ocean off the coast of South America.

Many thanks to NOAA/NESS and NOAA/NMFS for the use of their data. Special thanks to LT Craig Nelson, NOAA, for help on the plotting end.

The author is extremely indebted to FNWC for the use of their wind data and their computer.

The assistance of J. B. Wickham and R. L. Haney as advisors was invaluable.

I. INTRODUCTION

The meteorological and oceanographic activity of the Southern Hemisphere, although not nearly as widely studied as that of the Northern Hemisphere, is still of vital importance to the United States and the rest of the world. Its cause-and-effect impact on the weather and ocean situations of the North, as well as on vast resources there not well utilized, arouses scientific curiosity to understand the physical processes in the region.

One facet of these activities which is of particular interest is sea surface temperature (SST). This paper will attempt to determine if weekly averaged non-seasonal fluctuations of wind phenomena analyzed by Fleet Numerical Weather Central (FNWC) can be correlated with non-seasonal fluctuations of sea surface temperatures revealed by Global Operational SST Computation (GOSSTCOMP) data. The major eventual goal is to examine mechanisms responsible for synoptic scale fluctuations in SST. If changes in wind phenomena can be related to the changes in SST, then temperature inferred from wind fields may serve as a substitute for satellite data and possibly for prediction purposes.

The specific area studied for this report was the Eastern South Pacific, off the coasts of Ecuador, Peru, and Chile.

The wind phenomena chosen for correlation were perturbations of the vertical component of the curl of the wind stress ($curl_z \tau$) and friction velocity cubed (U_*^3). (Symbols used in this thesis are defined on the List of Symbols on page 9.) These parameters were used because the curl of Tau is responsible for Ekman convergence and divergence, and

frictional velocity is related to mixing. Both of these can be found to contribute to SST changes.

Meridional Ekman advection (as represented by Tau_x) could also be studied for relationship with SST, but it was not found to be practical with data used in this paper.

II. DEVELOPMENT OF BASIC THEORY INVOLVING U_*^3, CURL OF TAU, AND SST

Starting with the first law of thermodynamics,

1. $C_v \frac{dT}{dt} + P \frac{d\alpha}{dt} = \dot{H}$, where $\dot{H}$ is the rate of heating per unit mass.

Assuming incompressibility, then

$\frac{d\alpha}{dt} = 0$.

By expanding the total derivative of T and averaging it, while neglecting $\vec{V} \cdot \nabla_2 \bar{T}$ and $\nabla_2 \cdot (\overline{V'T'})$ (horizontal derivatives), we get

2. $\frac{\partial \bar{T}}{\partial t} + \overline{w}_e \frac{\partial \bar{T}}{\partial z} + \frac{\partial}{\partial z} (\overline{W'T'}) = \dot{Q}/\rho_{wo} C_v = R(z)$,

where R(z) is the absorption of solar radiation in the sea,

let $\dot{H} = \dot{Q}/\rho_{wo}$, and $\overline{W'T'}$ is proportional to the upward flux.

If we look at the mixed layer only, $\frac{\partial \bar{T}}{\partial z} = 0$, $\bar{T} = T_s$, and so (2) becomes

3. $\frac{\partial T_s}{\partial t} + \frac{\partial}{\partial z} (\overline{W'T'}) = R(z)$ with $z > -h$.

Next integrate equation 3 in depth from the surface to z = -h and neglect R(z), then

4. $\int_{-h}^{o} \frac{\partial T_s}{\partial t} dz = -[(\overline{W'T'})_o - (\overline{W'T'})_{-h}]$ which leads to

5. $\int_{-h}^{o} \frac{\partial T_s}{\partial t} = -(\overline{W'T'})_o + (\overline{W'T'})_{-h}$

Then with strong winds it would be expected that $(\overline{W'T'})_o$ (which is proportional to U_* multiplied by the air sea temperature difference) be larger and $(\overline{W'T'})_{-h}$ (which is proportional to U_*^3) be more negative (Figure 1). Thus, enhanced upward flux at the surface and downward flux at -h would result in lowering the SST.

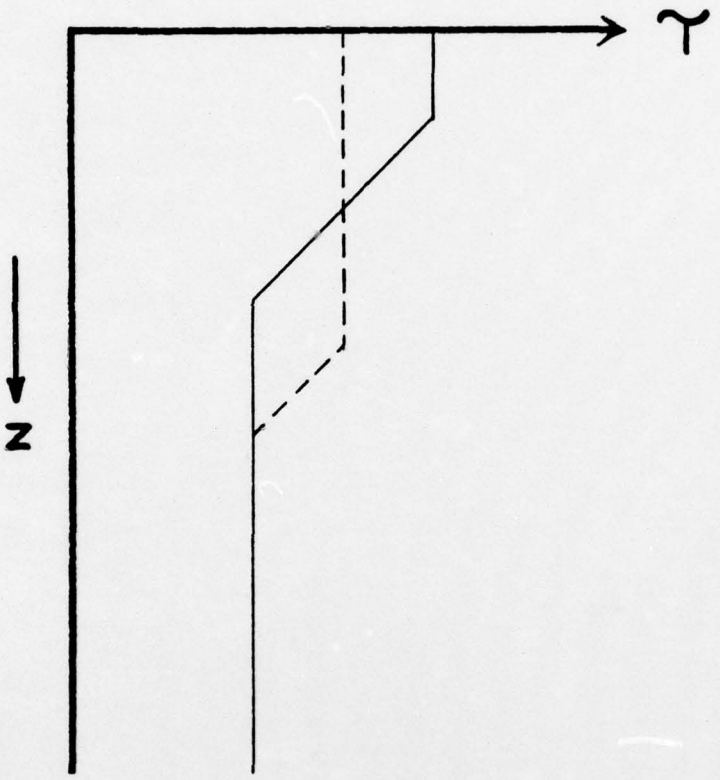

Figure 1. Influence of wind stress (τ) on ocean temperature (T) structure with depth. Solid line represents structure before U_* changed mixed layer. Dashed line represents resulting temperature profile after being effected by strong wind stress. Note how the mixed layer has lowered the surface temperature and increased the depth of the mixed layer.

In the equation (2) if $\frac{\partial \bar{T}}{\partial t}$ is not zero, there will be an effect of vertical advection. $\overline{W_e}$ is the mean vertical Ekman velocity and is directly related to the vertical component of the $curl_z\ \tau$.

6. $\overline{W_e} = \frac{1}{\rho_w f}\ curl_z\ \bar{\tau}$

In the Southern Hemisphere f is negative, and therefore, the current is directed 90° to the left of the wind. Also in the Southern Hemisphere where the winds in highs and lows rotate in opposite directions to that of the Northern Hemisphere, there is horizontal Ekman convergence and sinking motion within a surface counter-clockwise circulation and horizontal Ekman divergence and rising motion within a surface clockwise circulation. With this convergence, associated warming should be expected when the sign of $curl_z\ \tau$ is positive. Conversely clockwise circulation should have divergence yielding cooling with curl of Tau being negative. This process of surface diverging (converging) producing cooler (warmer) water has been called Ekman pumping (Figure 2).

The purpose of this thesis was to try to detect wind mixing (U_*^3) and/or Ekman pumping ($curl_z\ \tau$) from FNWC wind data and the GOSSTCOMP data.

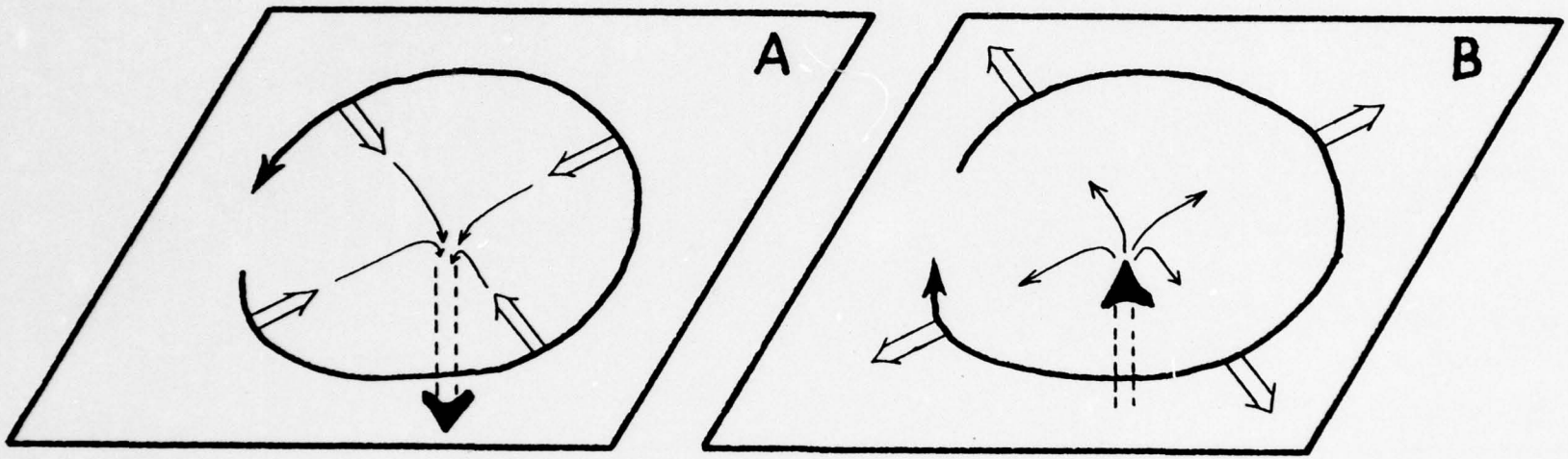

Figure 2. Diagram of the $curl_z \tau$ in the Southern Hemisphere

A. Counter clockwise circulation of the wind produces convergence; hence downwelling of the water (dashed arrow) resulting in sea surface warming.

B. Clockwise circulation of the wind produces divergence; hence upwelling of the water (dashed arrow) resulting in sea surface cooling.

III. DATA

Sea surface temperature observations were obtained from National Oceanic and Atmospheric Administration/National Environmental Satellite Service (NOAA/NESS)'s GOSSTCOMP datum.

The GOSSTCOMP data was a NOAA satellite scanning radiometer product which had been modified and composited in time. A detailed description of this product is found in NOAA/NESS Technical Memorandum #78, June '76. During the time frame of this report, past SST information (climatology) was used as one type of validity check.

This data was supplied weekly by NOAA/NESS through Defense Mapping Agency--Inter-American Geodetic Survey (DMA-IAGS), Canal Zone, on computer print-out paper.

The area of interest was from the coast of South America to 100°West longitude, and from the Equator to 40° South latitude. SST was displayed in tenths of a degree every one-half degree of latitude and longitude along with a confidence factor for that area.

For the purpose of the study, SST's were picked manually every 2 1/2° latitude and longitude in order to smooth the field, to relate it to wind data at every 2 1/2°, and, finally, to allow a reasonable time in card punching for computer graphics. Thus a SST field covering the area studied was produced for a period beginning 22 May 1974 and ending 28 May 1975, with a total of 53 maps.

Marine surface wind observations came from FNWC global band mercator maps. This data covered the Northern Hemisphere up to 60° North and the

Southern Hemisphere to approximately 40° South. Every 12 hours wind fields of surface "u" component and "v" component of wind in centimeters per second for the time frame of the report were made available in tape form for this study courtesy of FNWC. (Thesis data available from J. B. Wickham, Department of Oceanography, NPS).

The winds andtemperatures were defined at grid points which were equally spaced on the mercator projection and had to be converted to an equally spaced latitude-longitude (2 1/2°) grid. To do this, FNWC's Bessel interpolation scheme was used.

For the purpose of comparison, mean monthly SST maps came from Fishing Information (1974-1975), a publication of National Marine Fisheries Service (NMFS). Furthermore, the NMFS also supplied data from the El Niño Watch Cruise (11 February 1975 to 27 May 1975).

IV. PROCESSING OF DATA

Using the wind field tapes supplied by FNWC, the wind stress ($\vec{\tau}$) was calculated by the following equation, which involved two assumed constants,

7. $\vec{\tau} = \overrightarrow{\tau au} = \rho_a C_d |V| \vec{V}$.

For practical use this can be separated into components

$$\tau_x = \rho_a C_d (u^2 + v^2)^{1/2} u \quad \text{and}$$

$$\tau_y = \rho_a C_d (u^2 + v^2)^{1/2} v ,$$

where the density of air, ρ_a , is .00122 gm/cm^3, and the drag coefficient, C_d , is .0013.

The τ_x and τ_y fields were calculated every 12 hours and then averaged for seven days. The last date used in calculating the average corresponded to a given SST data date.

The main interest in this data was to be able to calculate the mean vertical component of the curl of Tau and mean U_*^3. It is believed that the changes in SST can be related by equation 2, as noted in another section

2. $$\frac{\partial \bar{T}}{\partial t} = - \overline{W_e} \frac{\partial \bar{T}}{\partial z} - \frac{\partial}{\partial z} (\overline{W'T'})$$

(1) (2) (3)

where term 1 is the change of mean temperature with time, term 2 is proportional to the curl of Tau, and term 3 is proportional to wind mixing.

The definition of friction velocity is

8. $U_* = \left(\frac{|\vec{\tau}|}{\rho_a}\right)^{1/2}$ (Glossary of Meteorology, 1959)

which leads to

9. $\bar{U}_*^3 = \left(\frac{(\bar{\tau}_x^2 + \bar{\tau}_y^2)^{1/2}}{\rho_a}\right)^{3/2}$.

The finite difference form of the vertical component curl of Tau equation in spherical coordinates over a seven day average is

10.

$$\vec{k}\cdot(\nabla\times\vec{\bar{\tau}}_{ij}) = \frac{1}{R\cos\phi_{ij}}\left[\left(\frac{\bar{\tau}_{yi+1,j}-\bar{\tau}_{yi-1,j}}{2\Delta\lambda}\right) - \left(\frac{(\bar{\tau}_x\cos\phi)_{i,j+1} - (\bar{\tau}_x\cos\phi)_{i,j-1}}{2\Delta\phi}\right)\right]$$

R is the radius of earth in centimeters.

$\Delta\lambda$ and $\Delta\phi$ equals the grid spacing which is 2 1/2° converted to radians.

ϕ is the latitude in radians.

$\bar{\tau}_x$ is the west to east component of wind stress averaged over a seven day period.

$\bar{\tau}_y$ is the south to north component of wind stress averaged over a seven day period.

$\vec{k}$ The vector $\vec{k}$ is a unit vector directed vertically.

These equations were incorporated into an existing program for calculating mean $\bar{\tau}_x$'s and $\bar{\tau}_y$'s. The results indicated that the curl Tau was of the magnitude 10^{-7} -- 10^{-8} dyne/cm^3, comparable to that of Hantel (1970), which was 2.3×10^{-8} dyne/cm^3, and the cube of the friction velocity (U_*^3) was of the magnitude of 1×10^4(cm/sec)^3.

The next step was to separate these seven day averaged fields into mean and perturbation values for the purpose of removing the seasonal

cycle. Using the basic equation $A = \bar{A} + A'$ where $\bar{A}$ is the mean and A' is the deviation of A from the mean, the weakly mean field was used to develop the annual mean field of each parameter (Figures 3, 4, 5). Once mean fields were generated, they were subtracted from the original field as shown by equations below

(with: i = number of days in a week and
j = number of weeks in a year)

$$(\text{curl}_z\ \tau)' = \text{curl}_z\ \tau - \left[\frac{1}{52}\sum_{j=1}^{52}\left(\frac{1}{7}\sum_{i=1}^{7}(\text{curl}_z\ \tau)_i\right)_j\right]$$

$$(\text{curl}_z\ \tau)' = \text{curl}_z\ \tau - \overline{\text{curl}_z\ \tau}$$

$$(U_*^3)' = U_*^3 - \left[\frac{1}{52}\sum_{j=1}^{52}\left(\frac{1}{7}\sum_{i=1}^{7}(U_*^3)_i\right)_j\right]$$

$$SST' = SST - \left[\frac{1}{52}\sum_{j=1}^{52}(SST)_j\right]$$

$$SST' = SST - \overline{SST}$$

The perturbation fields of the $\text{curl}_z\ \tau$, friction velocity cubed, and sea surface temperature were put into contoured map form so that their spatial variations could be examined. From an examination of these maps a decision was made to concentrate the study on the mid-latitude regions. A line of data from 27.5° South to 39.5° South at 87.5° West was chosen because it was thought to be far enough from the coast to eliminate coastal effects and close enough at mid-latitude to be under the effect of mid-latitude storms.

On this North-South line, consisting of five stations (Figure 6) separated by 2 1/2° latitude, the seven-day average SST's were plotted for May 1974 to May 1975 (Figures 7A, 8A, 9A). A definite sinusoidal

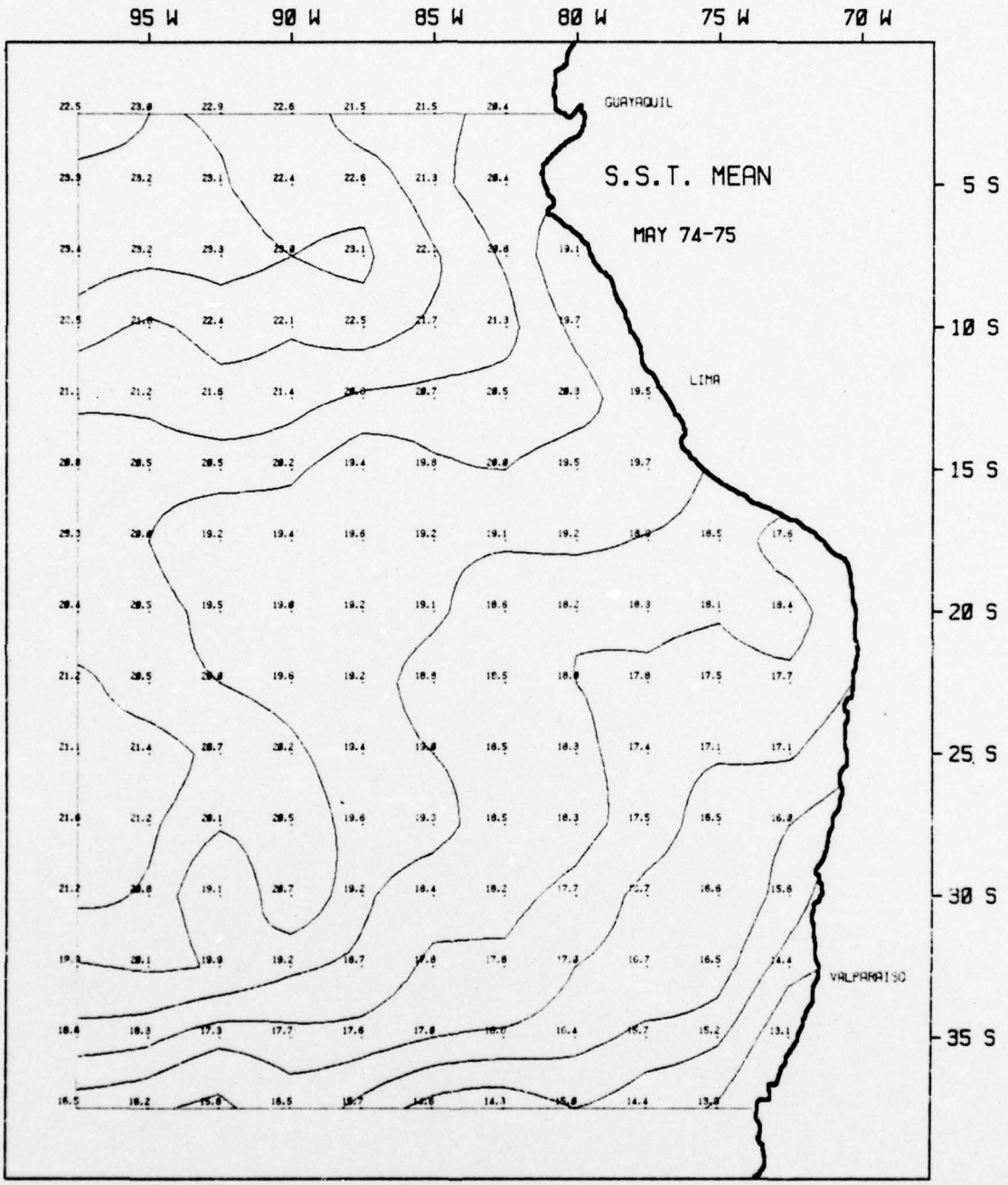

Figure 3. Annual mean sea surface temperatures (°C) from 28 May 74 to 28 May 75.

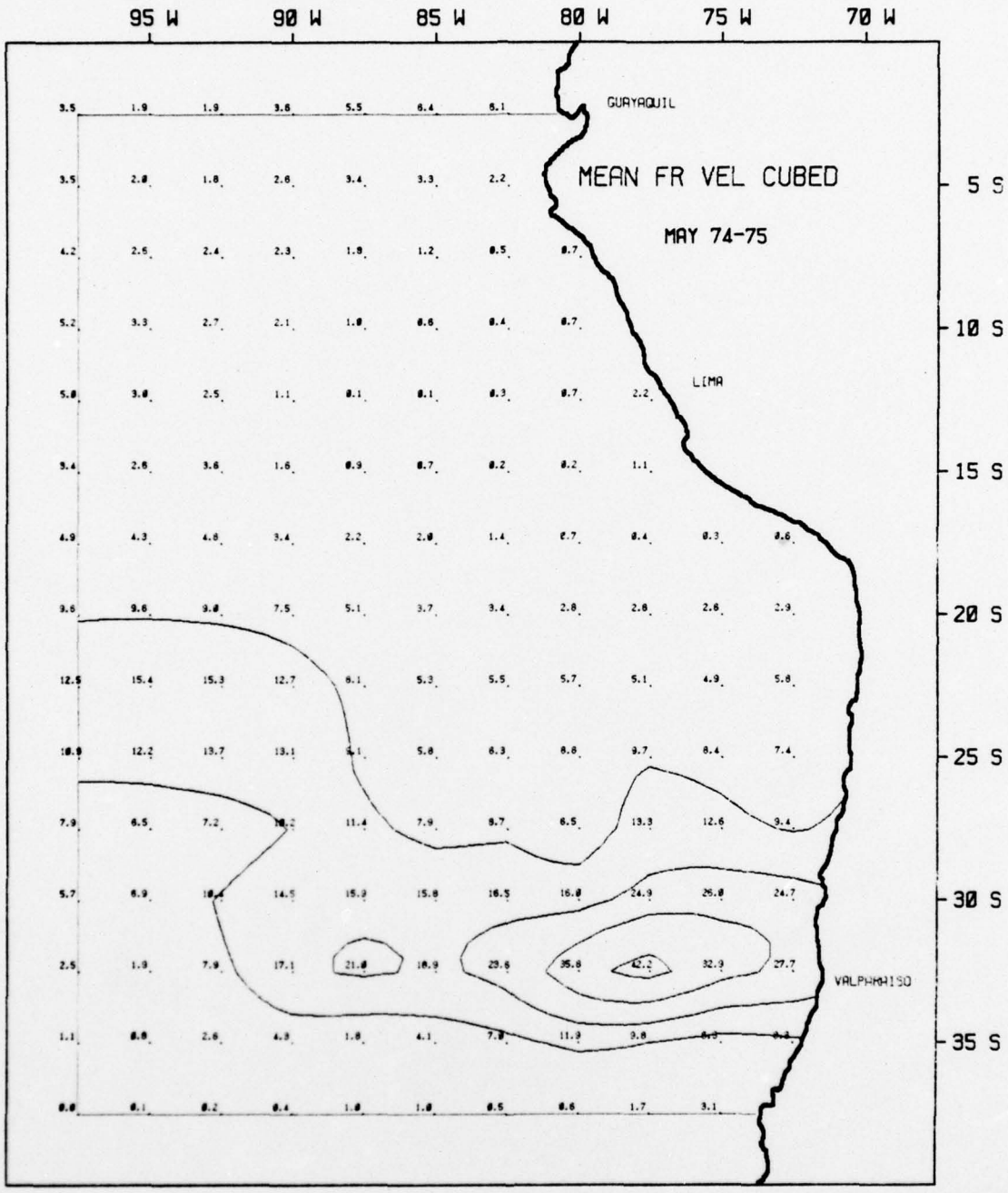

Figure 4. Annual mean friction velocity cubed in 10^3 cm/sec from 28 May 74 to 28 May 75.

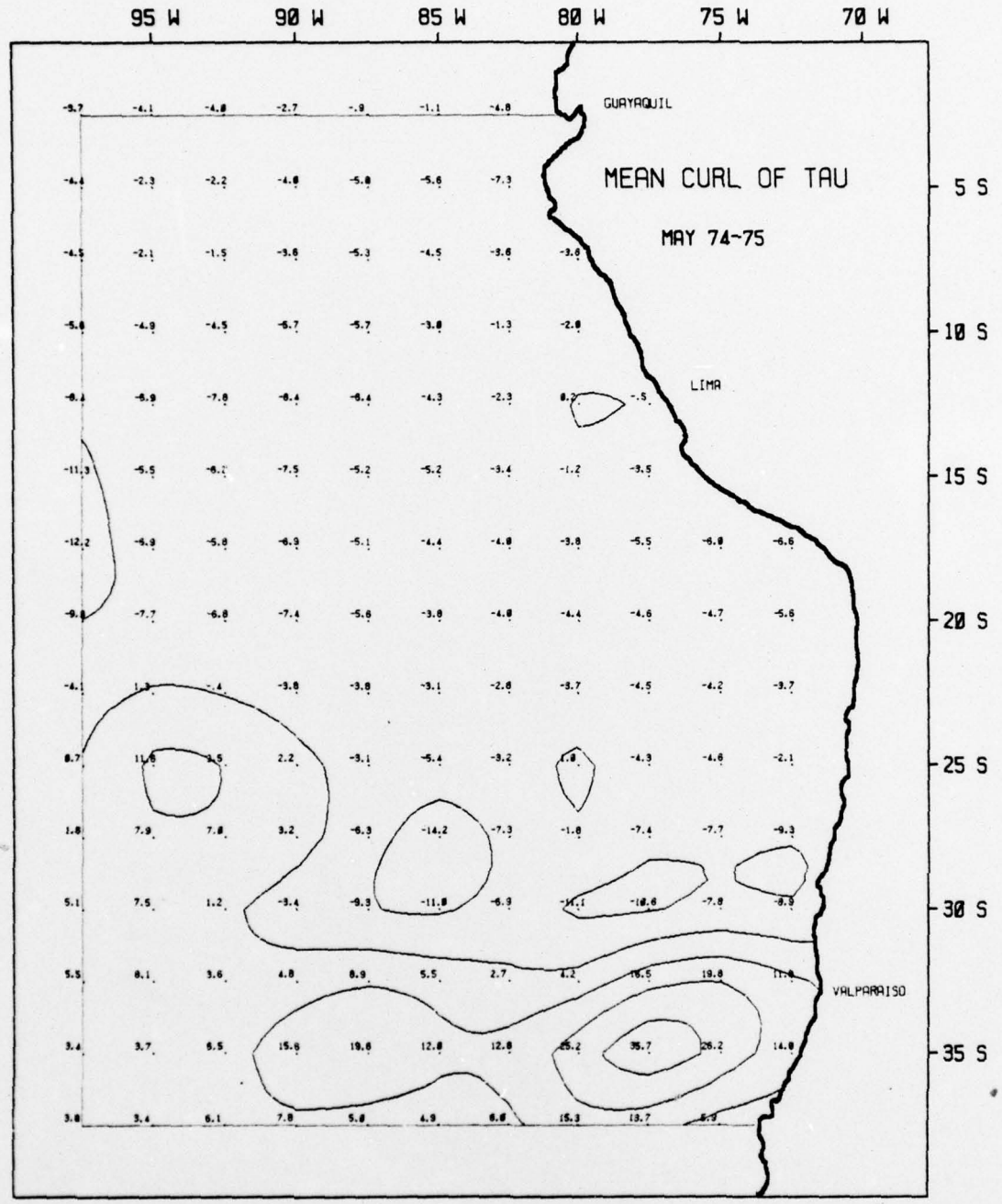

Figure 5. Annual mean $curl_z \tau$ in 10^{-9} dyne/cm^3 from 28 May 74 to 28 May 75.

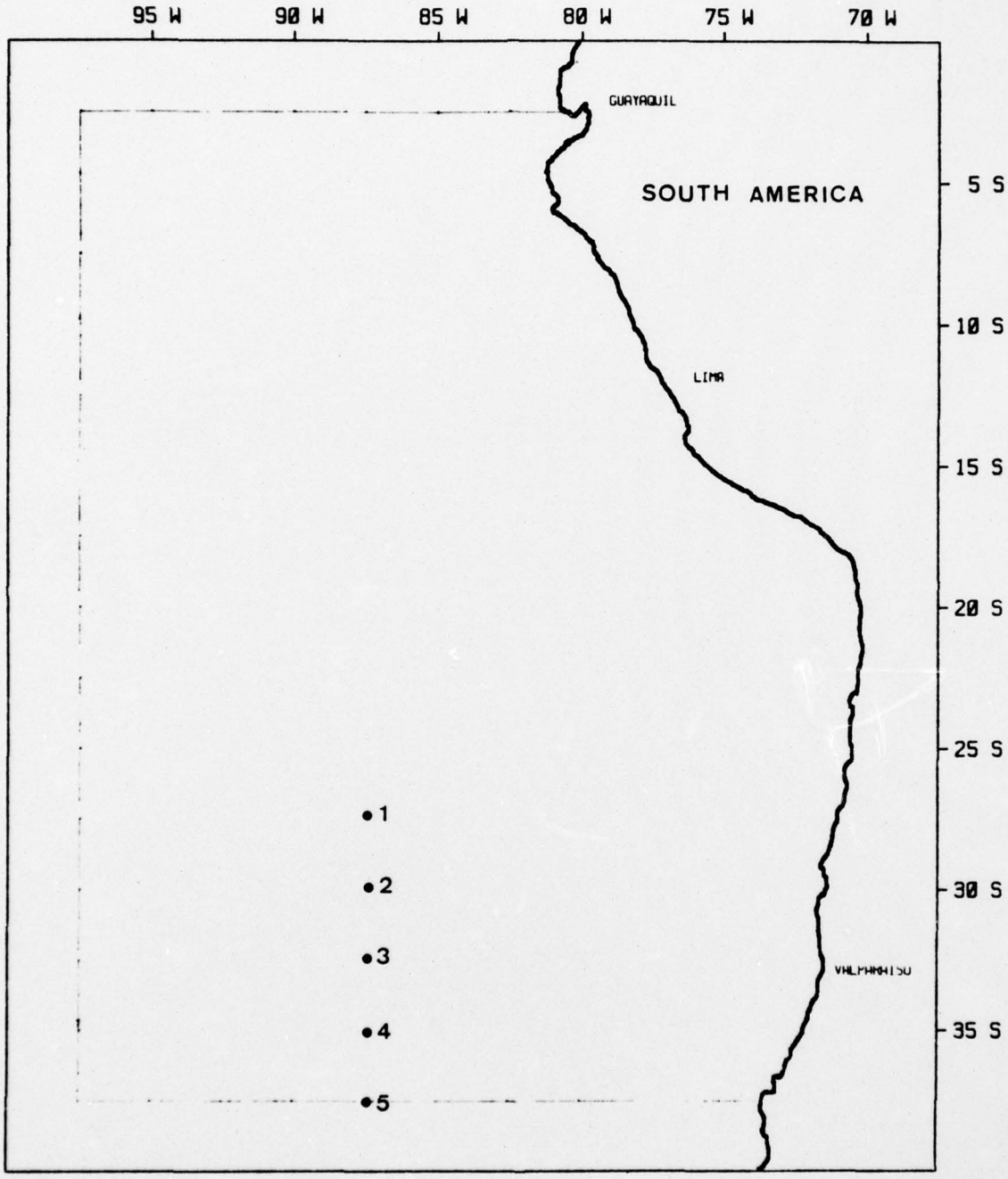

Figure 6. Location of the five sample points.

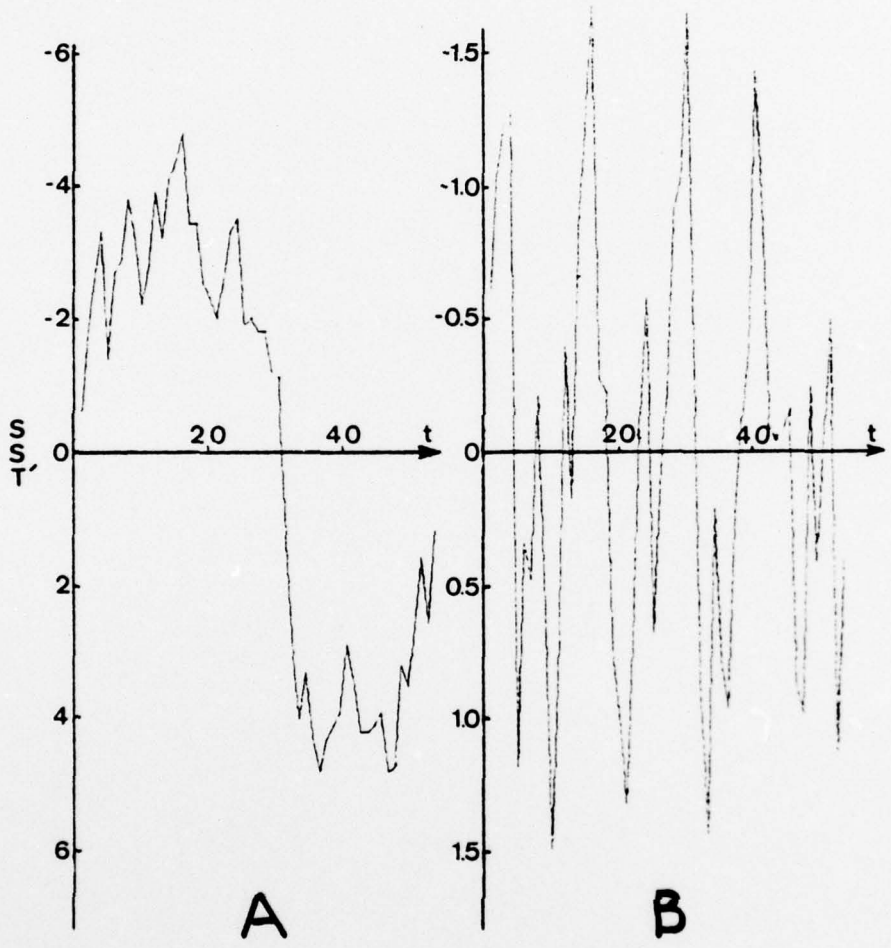

Figure 7. Weekly time (t) series for SST' for May 74 - May 75 at 32.5°N and 87.5°W (Station #3)
A. Represents the annual mean removed
B. Represents the seasonal cycle removed.

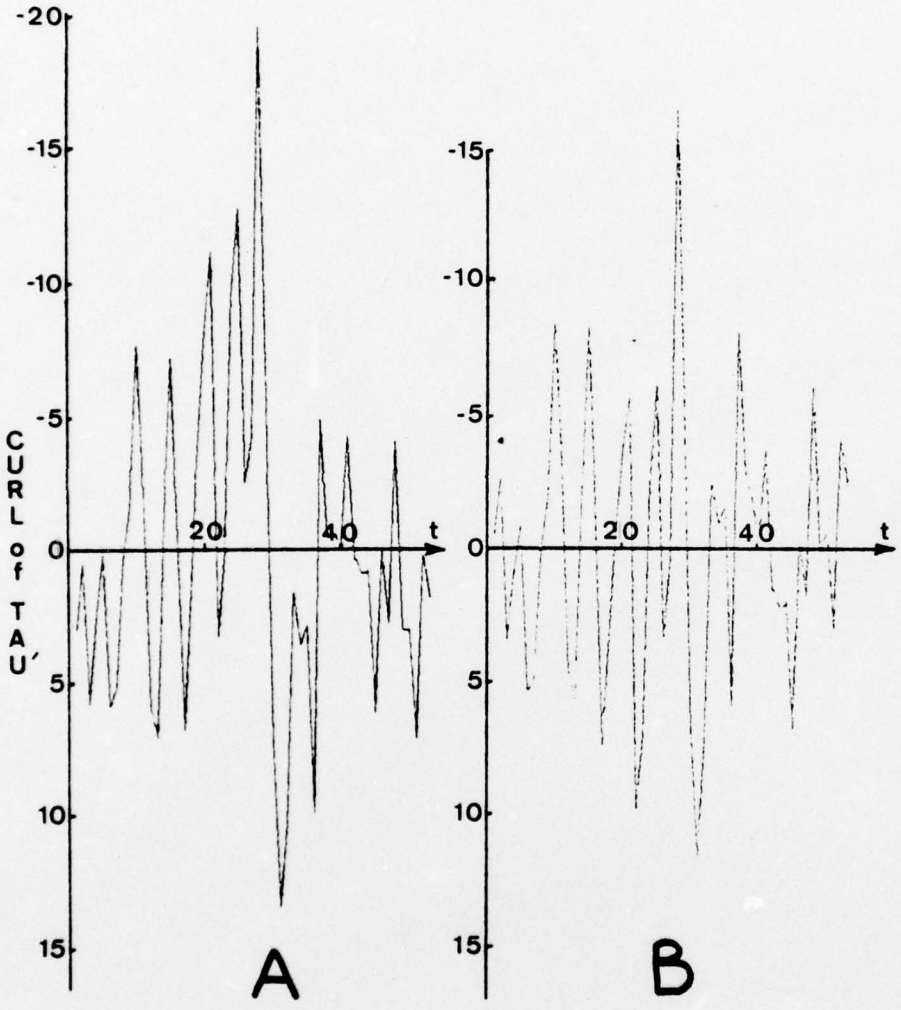

Figure 8. Weekly time (t) series for $(\text{curl}_z \tau)'$ for May 74 - May 75 at 32.5°N and 87.5°W (Station #3)
A. Represents the annual mean removed
B. Represents the seasonal cycle removed.

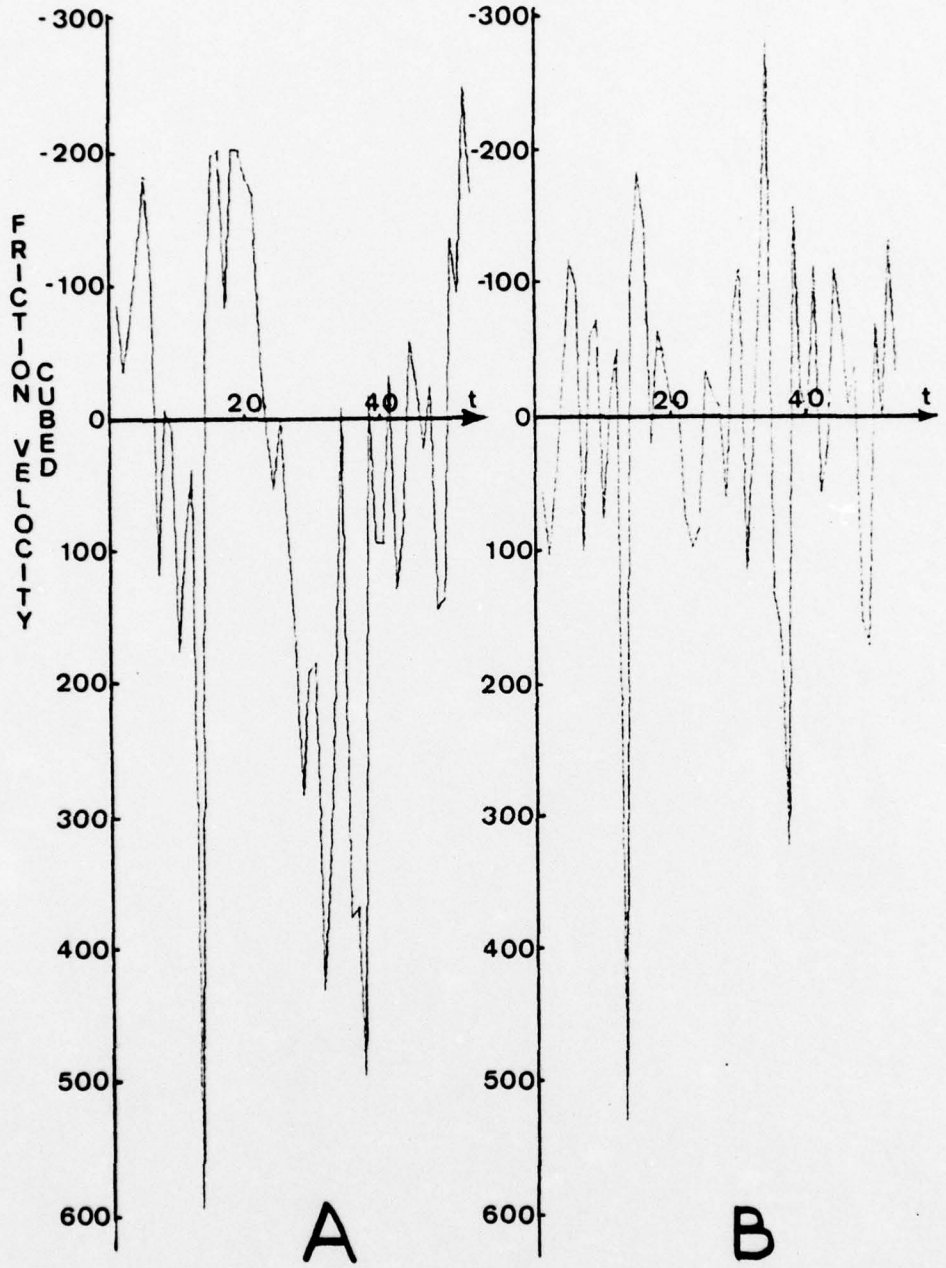

Figure 9. Weekly time (t) series for $(U_*^3)'$ for May 74 - May 75 at 32.5°N and 87.5°W (Station #3)
A. Represents the annual mean removed
B. Represents the seasonal cycle removed.

shape was obvious in the data, especially the SST. Therefore it was necessary to remove the seasonal effect since the interest of this study was the synoptic time scale perturbations.

Harmonic analysis of the data was done, and the mean and first three harmonics, eliminating the seasonal cycle, were removed, leaving the synoptic frequencies. This synoptic frequency part of the $(\text{curl}_z\ \tau)'$,$(U_*^3)'$, and SST' were then plotted in time series to verify that the seasonal effect had been removed (Figures 7B, 8B, 9B).

V. OBSERVATIONS

A. WARM SST TONGUE

A study of the sea surface temperature maps for the year period showed a very apparent tongue of warm water migrating from the North to the South near the coasts of Ecuador and Peru.

A moderately warm finger (17°C) began forming in September (Figures 10, 11, 12), sloping down from the northwest parallel to and about 5°S from the coast. It essentially remained stationary until November when it extended farther down the coast to about 20° South latitude. By the end of November the core was 18°C. At the end of December, the core warmed to 19°C and in January to 21°C. By February the maximum temperature was 23°C. The basic structure of this warm anomaly was still tongue-shaped from the North and extended to 20° South latitude. Its temperature decreased in March, and as May developed, the tongue vanished totally.

The change in temperature in this area (20°S, 75° West) was 8.4°C from 28 August 1974 (-3.8°C below mean) to 19 February 1975 (+4.6°C above mean). It would be difficult to attribute this SST difference wholly to seasonal change, or at least to the kind of seasonal change seen in neighboring areas which are notably smaller.

B. COMPARISON OF NOAA/NESS GOSSTCOMP DATA WITH THAT OF NOAA/NMFS MEAN MONTHLY SST MAPS

The products from NOAA/NESS GOSSTCOMP and NOAA/NMFS appeared somewhat similar. The NMFS usually ahd strong coastal gradients and North-South gradients at the equator. This was not shown on the GOSSTCOMP

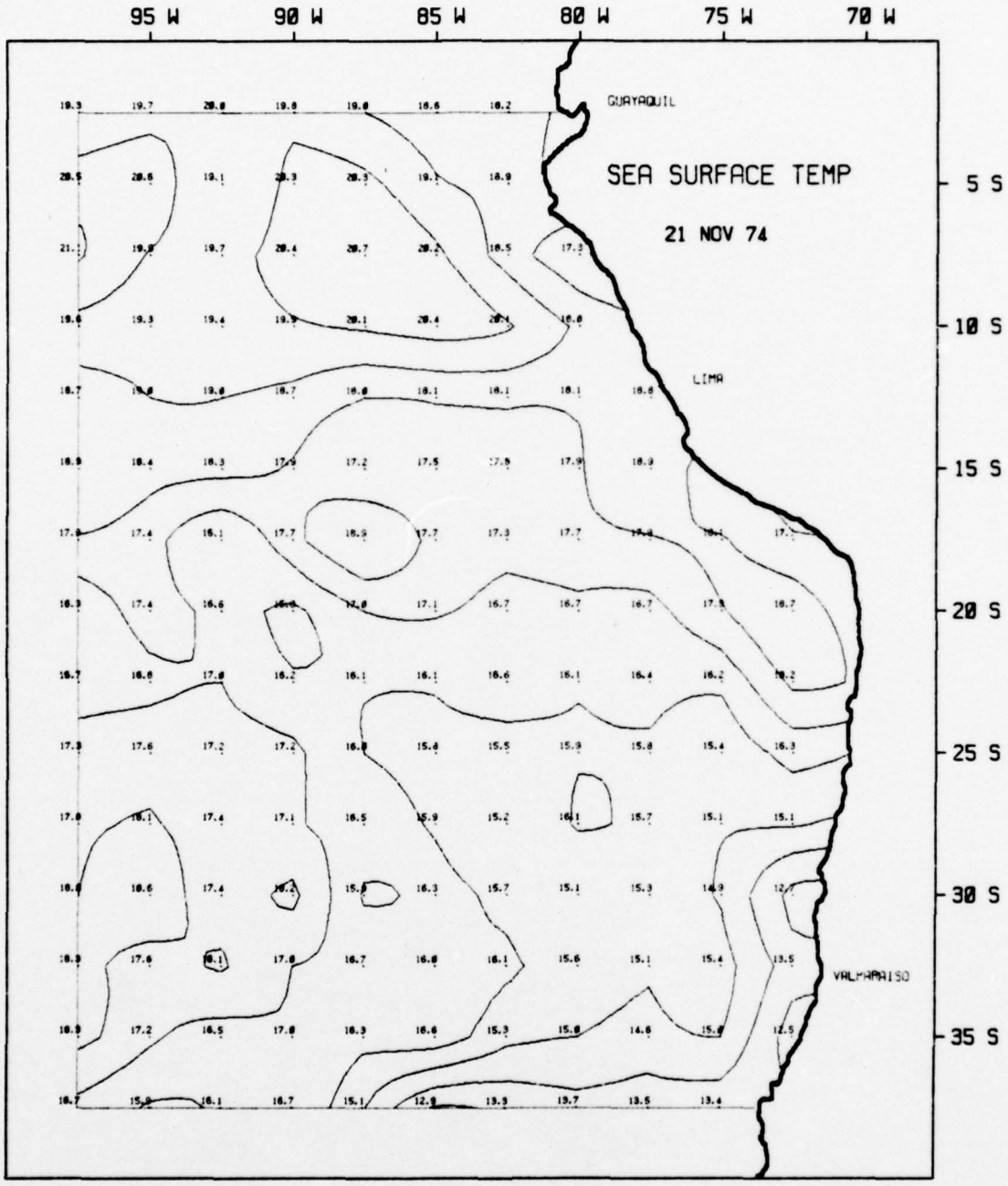

Figure 10. Sea surface temperatures (°C).

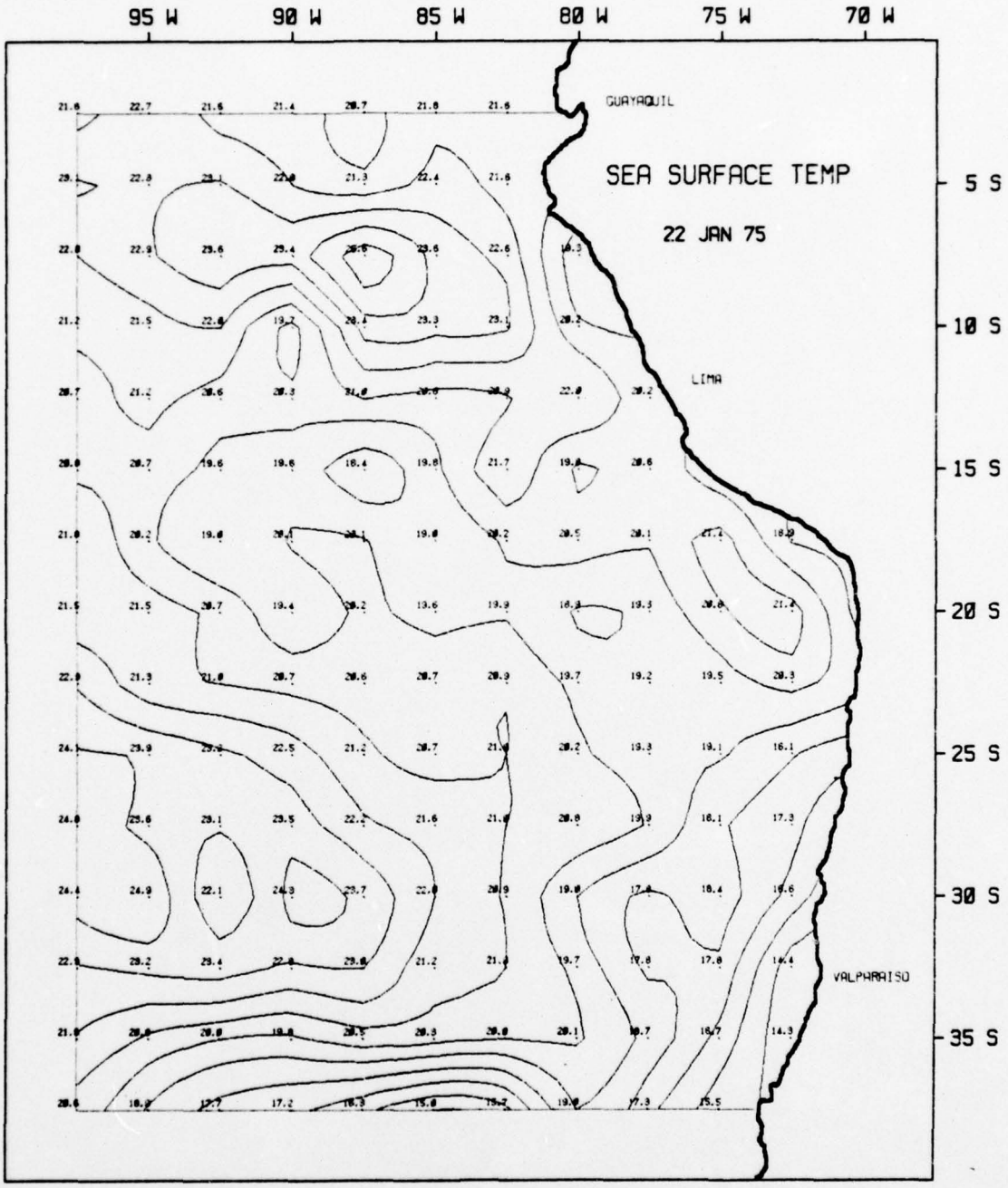

Figure 11. Sea surface temperatures (°C).

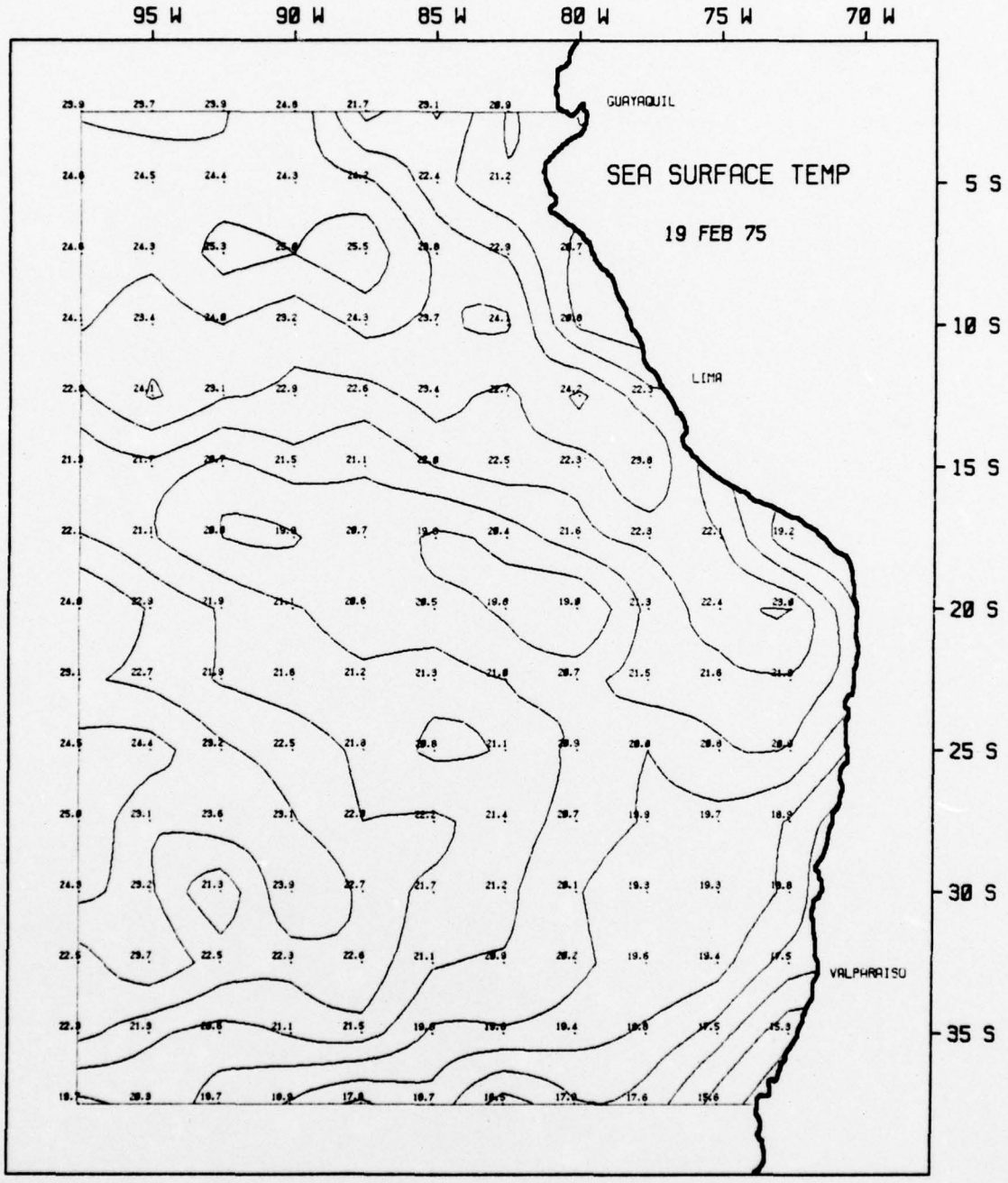

Figure 12. Sea surface temperatures (°C).

data. Some significant anomalies were observed in May and November on both products. The basic trends in the GOSSTCOMP data were depicted in the NMFS generally, though not always consistently.

It should be pointed out that the NMFS SST maps are means and did indicate that the data was sparse in this particular region. The GOSSTCOMP was an accumulated short time daily average.

C. COMPARISON OF SMOOTHED GOSSTCOMP DATA WITH DATA FROM EL NINO WATCH CRUISE, 11 FEB 75 to 27 MAY 75

This shipboard data was supplied by the NMFS from the University of Hawaii and the Scripps Institution of Oceanography investigation of El Niño (reference Wyrtki, et al. 1976). Data was extracted from this investigation that corresponded the closest in space and in time to available GOSSTCOMP data in the area of interest (Table I).

Of the several random examples selected for comparison, the average absolute difference between the cruise data and GOSSTCOMP data was 1.17°C. In NOAA/NESS TM 78, the indication for 0°-360° longitude from 20° South to 90° South was a mean absolute difference in ship measurement versus satellite measurements was 0.75°C. For the purpose of this study it was assumed that SST fluctuations equal to or greater than 1°C in the GOSSTCOMP data were an accurate representation of the ocean conditions.

D. SST' AND (CURL OF TAU)'

An observation of the maps of the deviation of the means indicated a relationship of ($curl_z \tau$) to SST'. As previously mentioned in the Southern Hemisphere with associated positive(negative) values of the ($curl_z \tau$)', Ekman convergence (divergence) leading to surface warming (cooling) can be expected. Four cases of Ekman pumping were selected from the synoptic maps and summarized in Table II. For example,

	Date	Location of Mona Wave	A Mona Wave SST (°C)	GOSSTCOMP Location	B GOSSTCOMP SST (°C)	B-A ΔT(°C)
1	26 Feb 75	14.00S 93.93W	22.77	15.0S 92.5W	22.2	-0.6
2	26 Mar 75	9.00S 85.93W	27.02	10.0S 85.0W	24.5	-2.5
3	23 Apr 75	4.77S 91.20W	27.00	5.0S 90.0W	25.4	-1.6
4	23 Apr 75	2.50S 92.56W	25.85	2.5S 92.5W	25.9	0.0
5	30 Apr 75	12.54S 91.91W	24.16	12.5S 90.0W	26.0	+1.8
6	30 Apr 75	13.96S 88.97W	22.86	15.0S 87.5W	22.1	-0.9
7	7 May 75	2.49S 86.00W	23.88	2.5S 85.0W	24.7	+0.8

Average Absolute Error = 1.17°C
Average Error = -.43

Table 1. Sample of El Niño Watch (Mona Wave) data vs. GOSSTCOMP data.

Case 1 30°S 90°W (warming)	11 Sept 74 SST' −5.1 $Curl_z\ \tau$ +11.8	19 Sept 74 SST' −3.6 $Curl_z\ \tau$ +63.	25 Sept 74 SST' −3.6 $Curl_z\ \tau$ +34.8	
Case 2 25°S 90°W (warming)	06 Nov 74 SST' −4.3 $Curl_z\ \tau$ +4.1	13 Nov 74 SST' −2.8 $Curl_z\ \tau$ +12.0		(Figures 13, 14, 15, 16)
Case 3 30°S 90°W (cooling)	12 Feb 75 SST' +4.9 $Curl_z\ \tau$ −2.3	19 Feb 75 SST' +3.5 $Curl_z\ \tau$ −22.5		(Figures 17, 18, 19, 20)
Case 4 35°S 80°W (warming)	12 Mar 75 SST' +3.7 $Curl_z\ \tau$ +12.5	19 Mar 75 SST' +4.9 $Curl_z\ \tau$ +22.9	26 Mar 75 SST' +4.5 $Curl_z\ \tau$ −1.0	

Table II. Summary of cases showing relationship in time between $curl_z\ \tau$ and SST'.

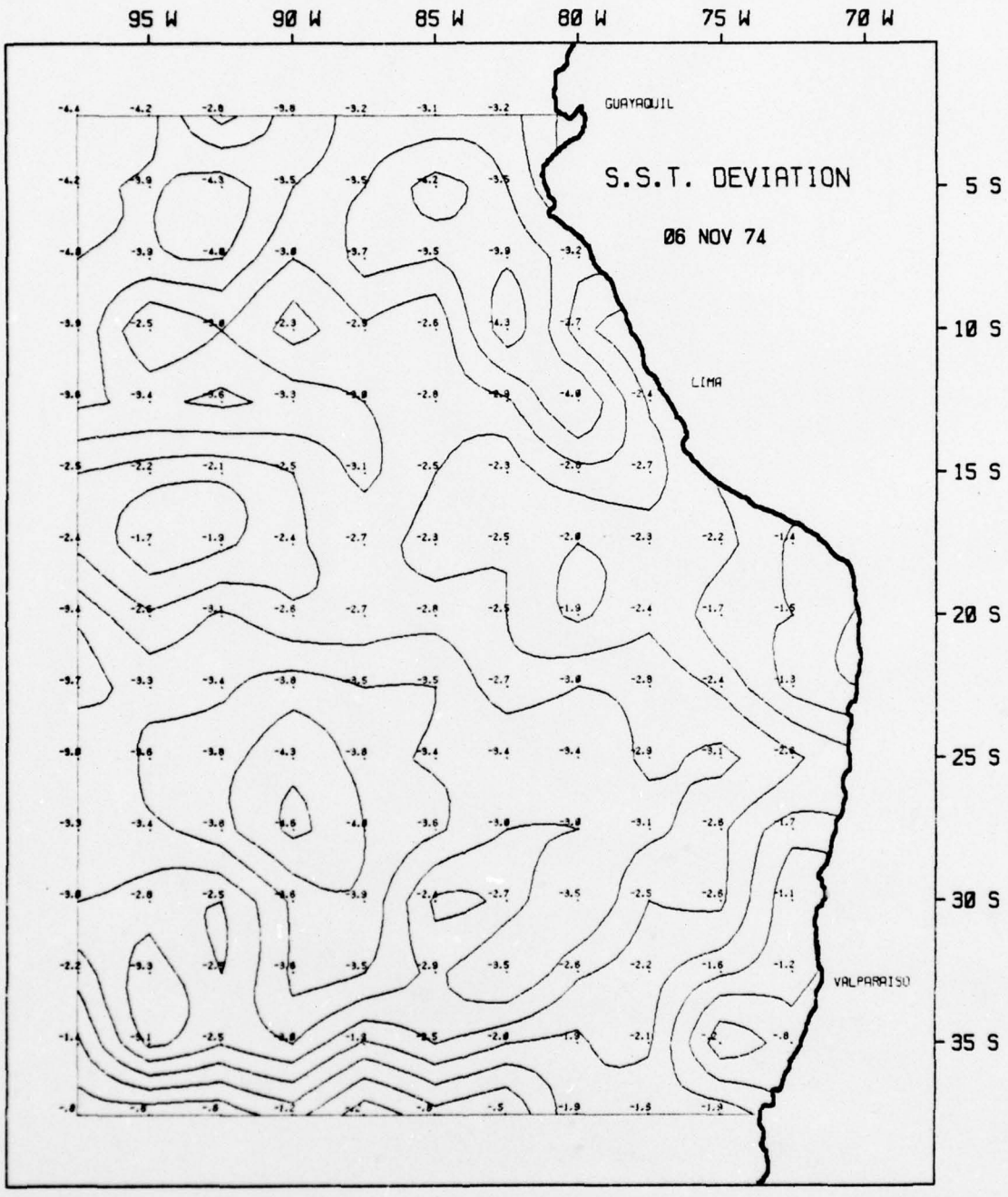

Figure 13. Sea surface temperature deviations from the mean in °C.

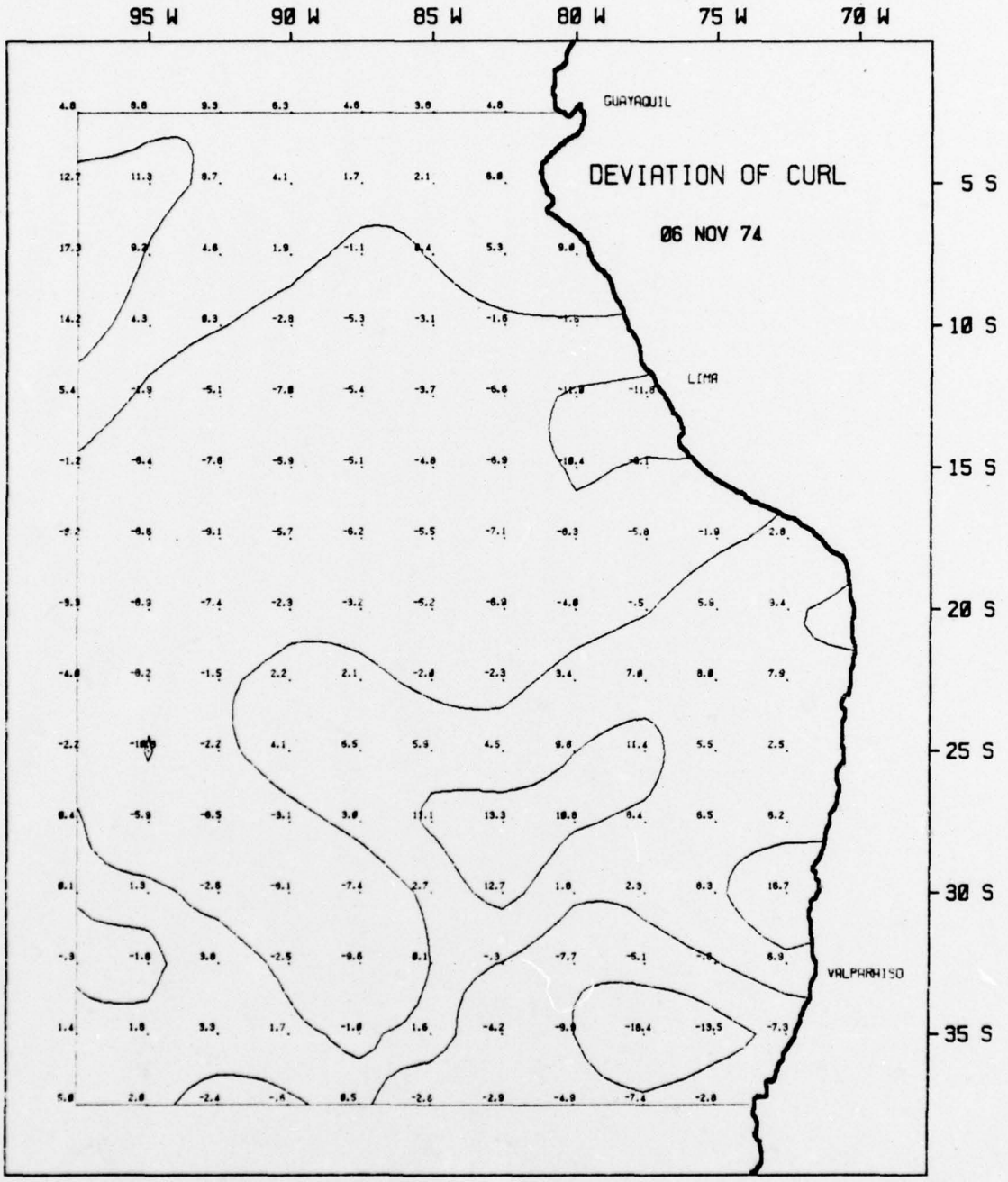

Figure 14. Deviations from the mean of $curl_z \tau$ in 10^{-9} dyne/cm^3.

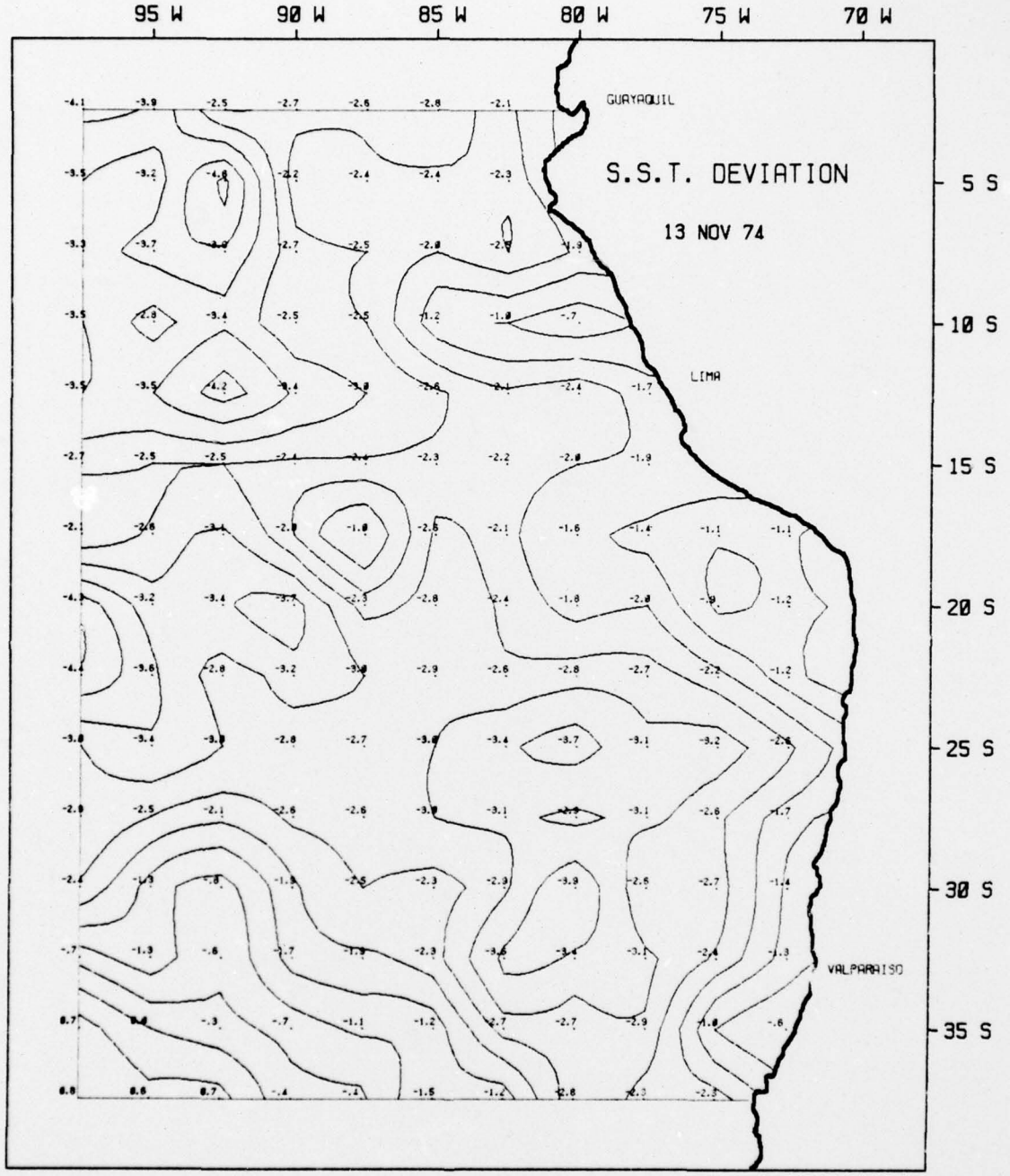

Figure 15. Sea surface temperature deviations from the mean in °C.

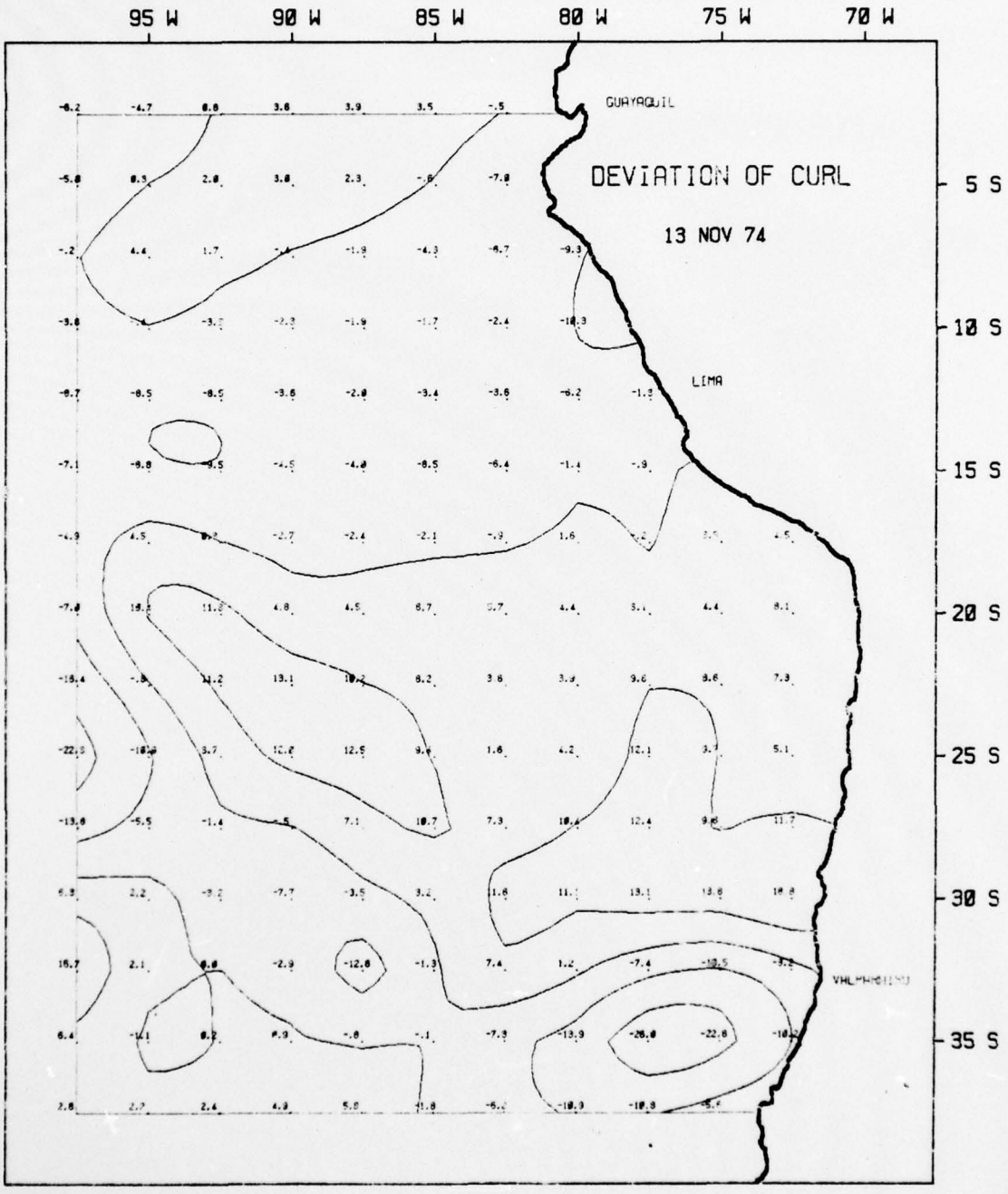

Figure 16. Deviations from the mean of $curl_z \tau$ in 10^{-9} dyne/cm^3.

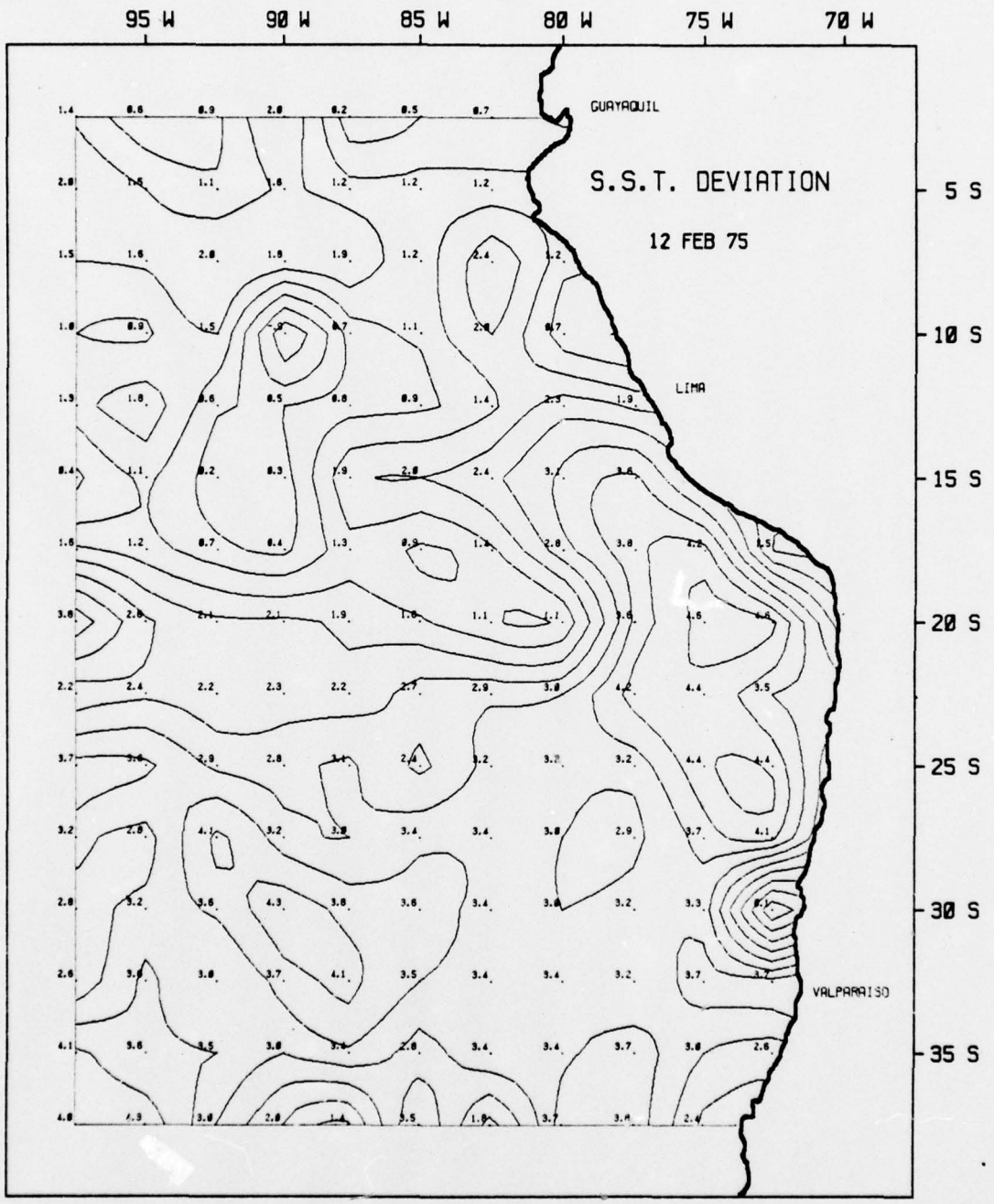

Figure 17. Sea surface temperature deviations from the mean in °C.

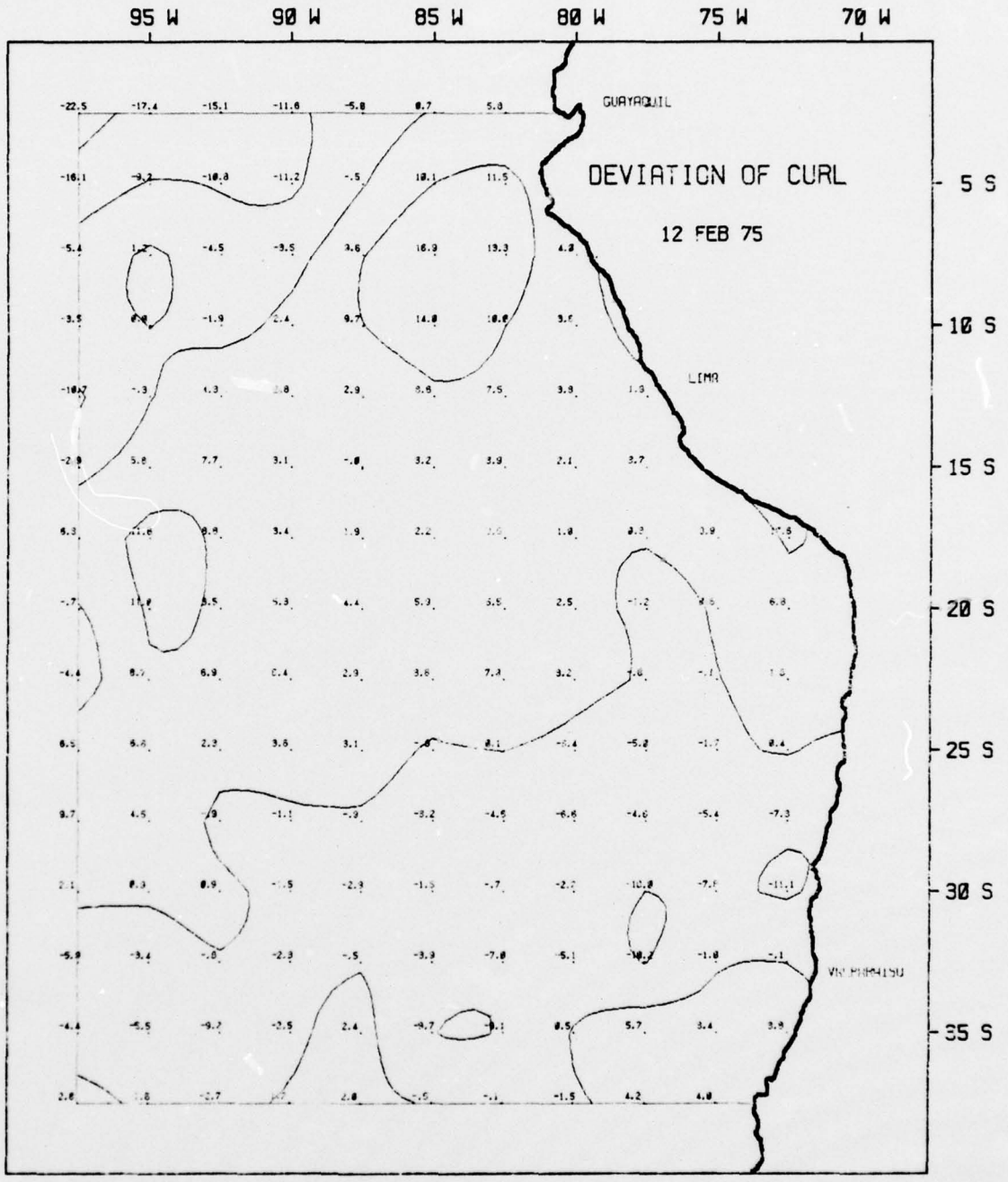

Figure 18. Deviations from the mean of $curl_z \tau$ in 10^{-9} dyne/cm^3.

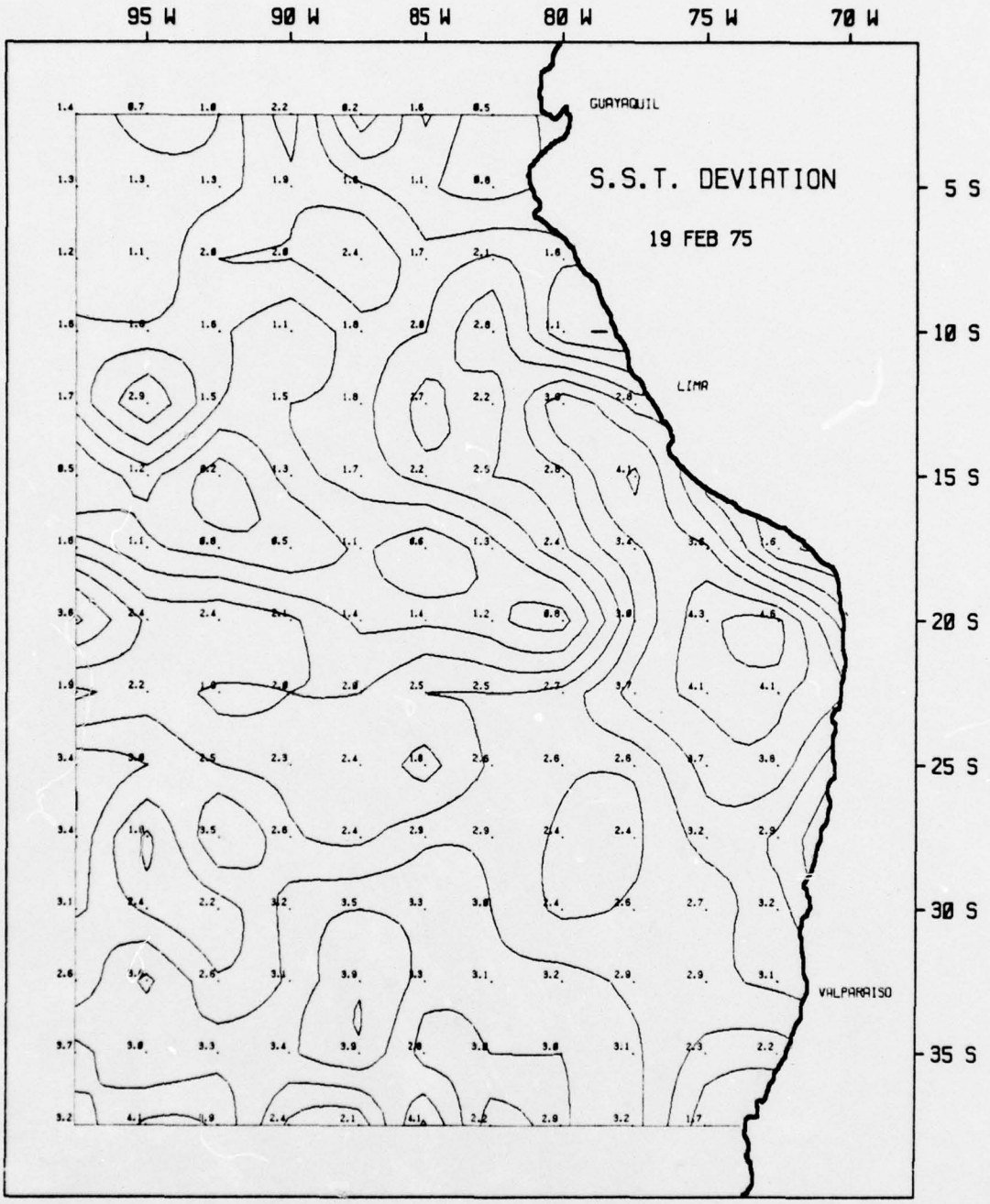

Figure 19. Sea surface temperature deviations from the mean in °C.

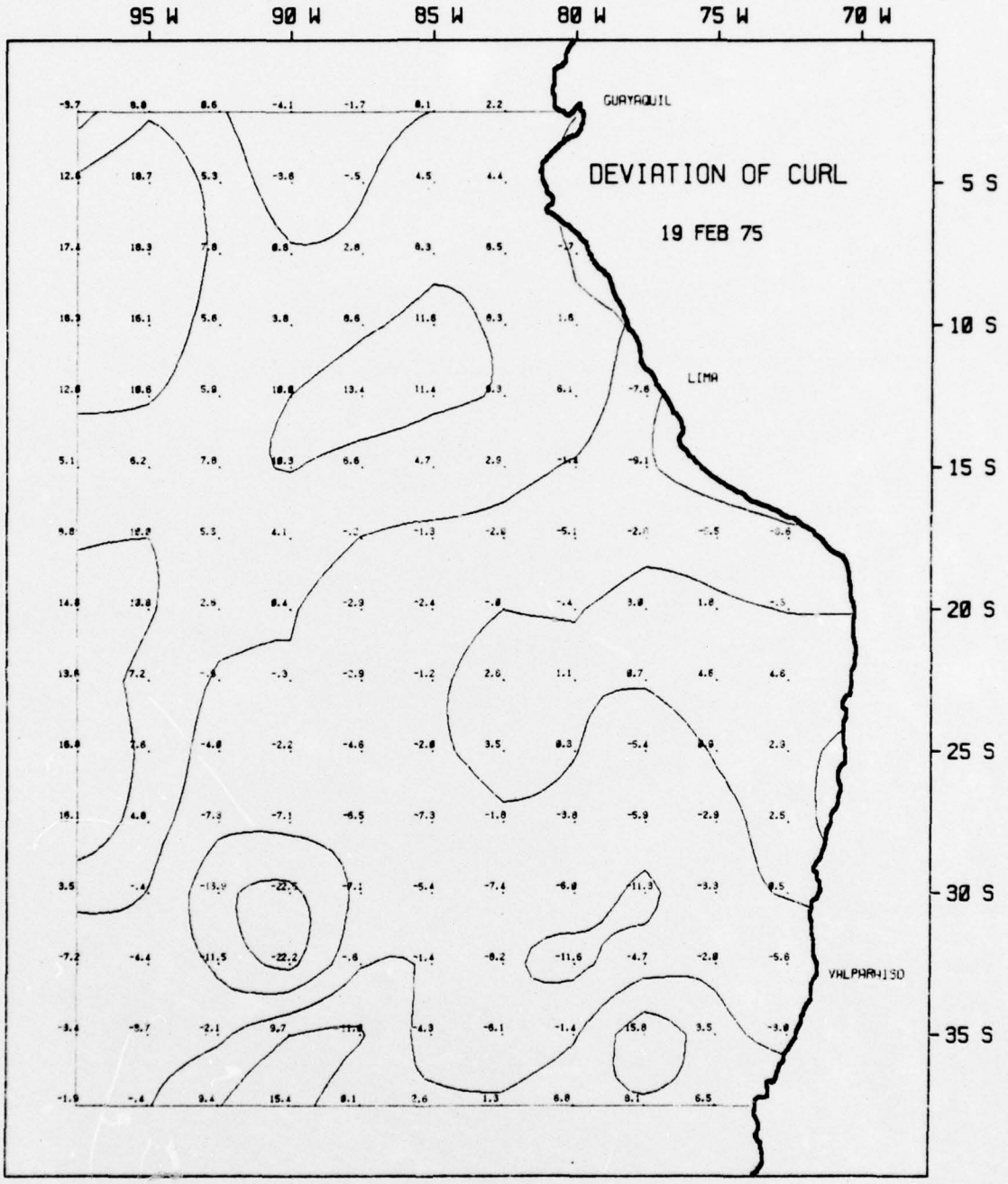

Figure 20. Deviations from the mean of $curl_z \tau$ in 10^{-9} dyne/cm^3.

in Case I, at 30°S, 90°W from 11 September 1974, to 25 September 1974, the $curl_z\ \tau$ anomaly was strongly positive and the SST' increased during this time period from -5.1°C to -3.6°C. The other three cases show a similar relationship.

E. SST' AND $(U_*^3)'$

An examination of the anomaly maps indicated a relationship of $(U_*^3)'$ to SST'. As this wind increased above normal (or mean), lower values of SST' were seen. Two cases of mixing were selected from the synoptic maps and summarized in Table III. For example, in Case I at 32.5°S, 75°W from 5 June to 19 June 1974, the U_*^3 anomaly was strong and the SST' decreased during this time period from +1.6°C to -2.7°C. The other case shows a similar relationship.

Case 1 32.5°S 75°W (cooling)	05 June 74 SST' +1.6 $(U_*^3)'$ +101	12 June 74 SST' -1.5 $(U_*^3)'$ +229	19 June 74 SST' -2.7 $(U_*^3)'$ +83
Case 2 32.5°S 85°W (cooling)	14 Aug 74 SST' -3.1 $(U_*^3)'$ +130	21 Aug 74 SST' -3.4 $(U_*^3)'$ +402	28 Aug 74 SST' -4.0 $(U_*^3)'$ -62

(Figures 21, 22, 23, 24, 25, 26)

Table III. Summary of two cases showing relationship in time between $(U_*^3)'$ and SST'.

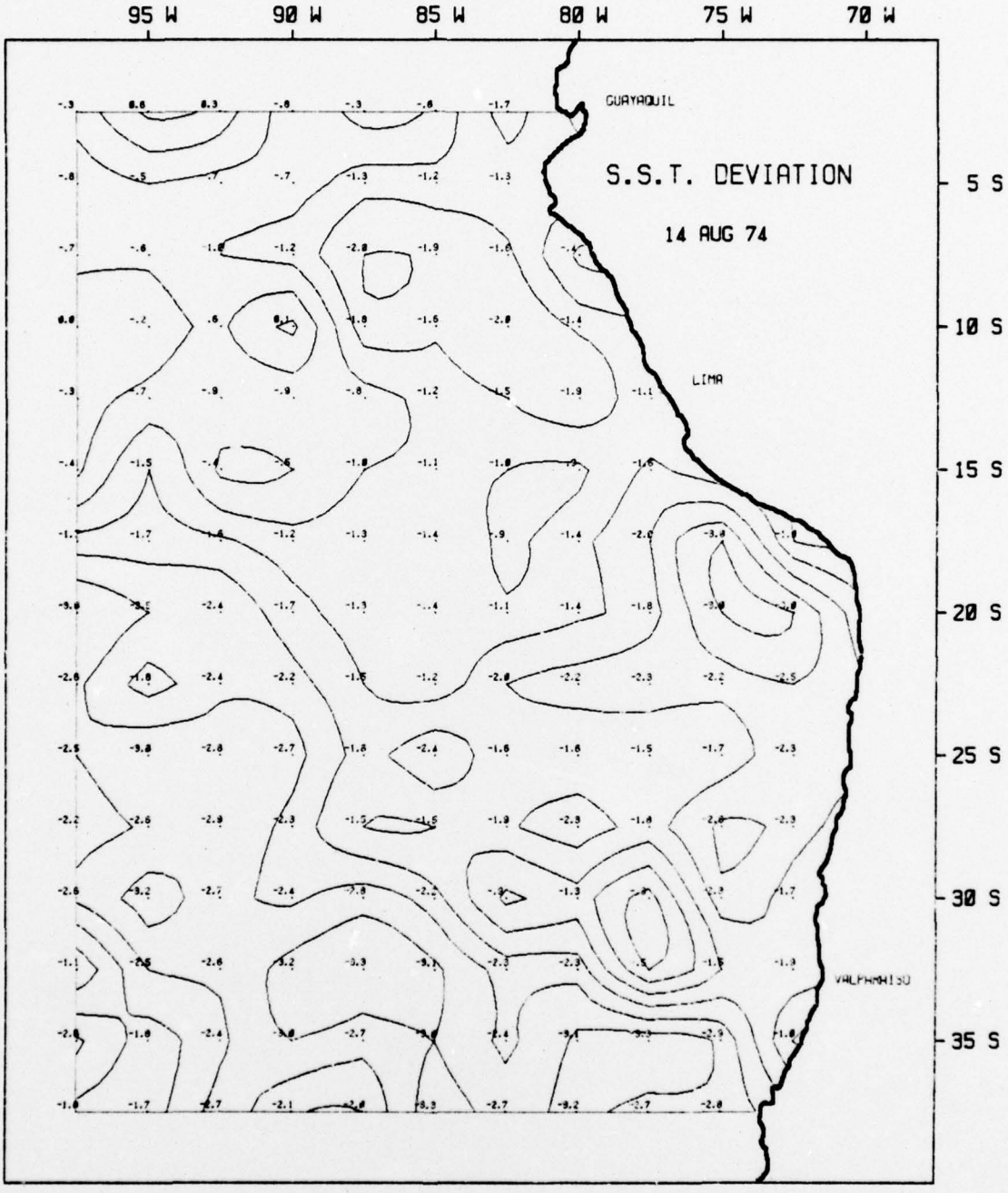

Figure 21. Sea surface temperature deviations from the mean in °C.

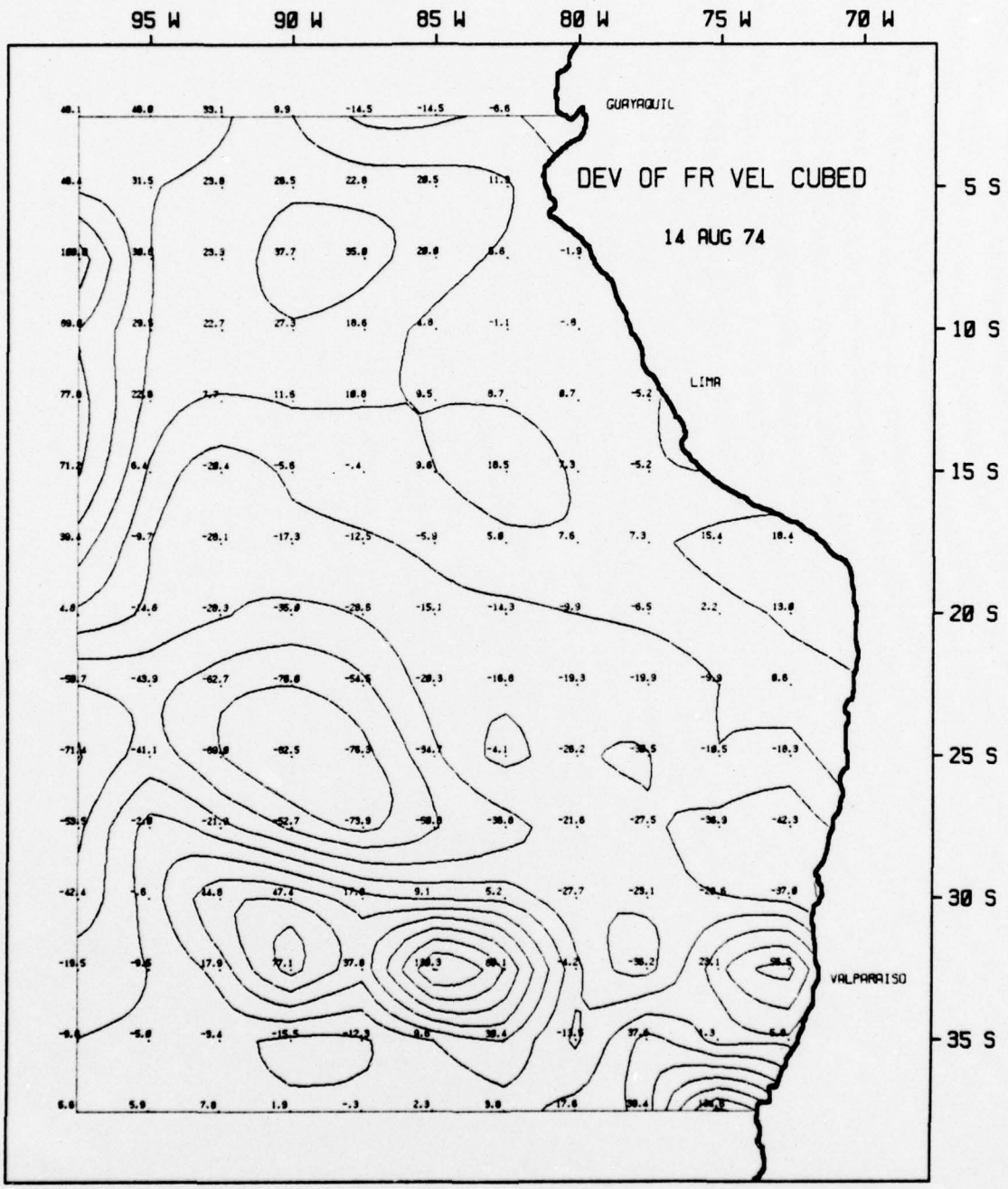

Figure 22. Deviations from the mean of U_*^3 in 10^2 cm/sec.

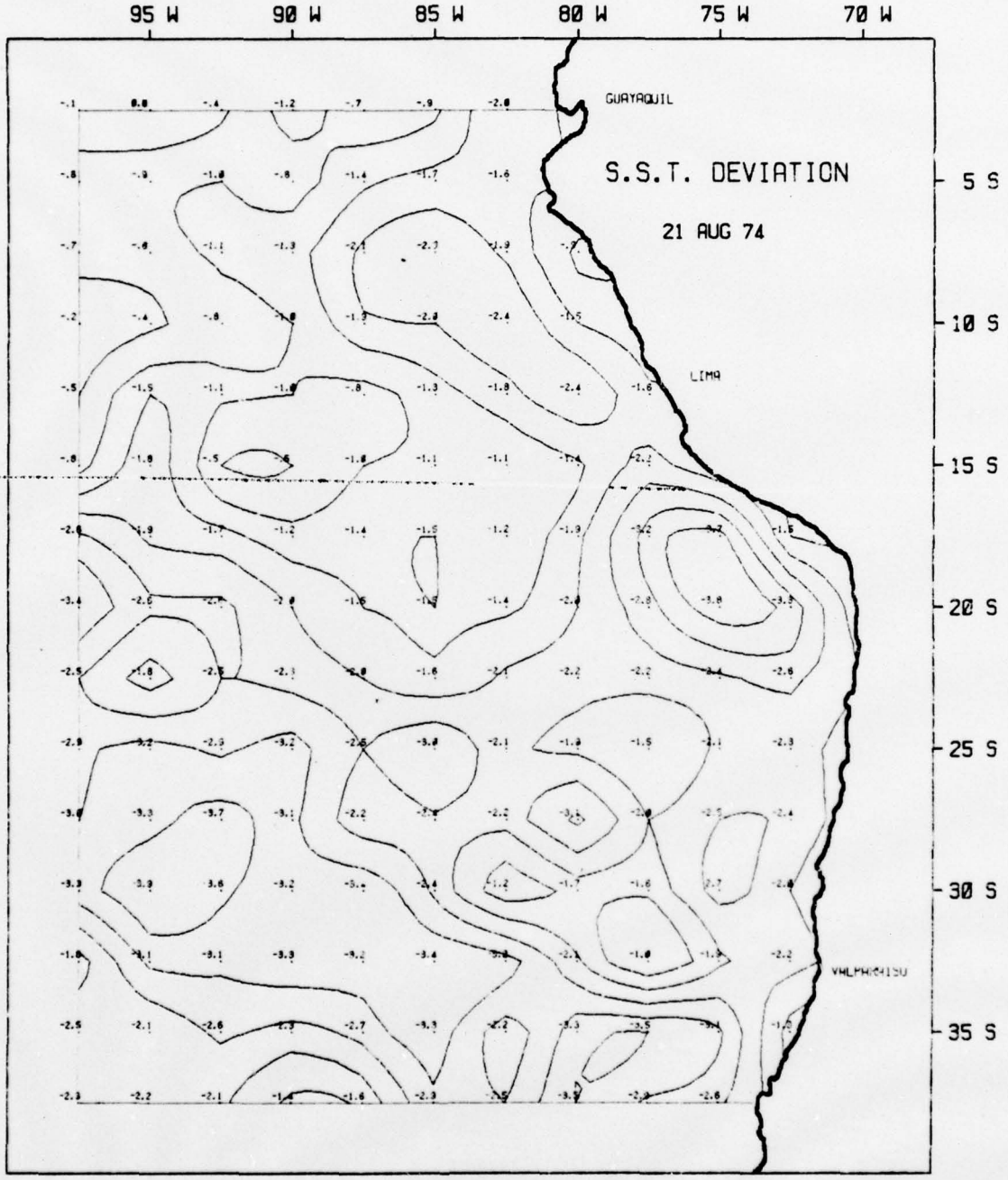

Figure 23. Sea surface temperature deviations from the mean in °C.

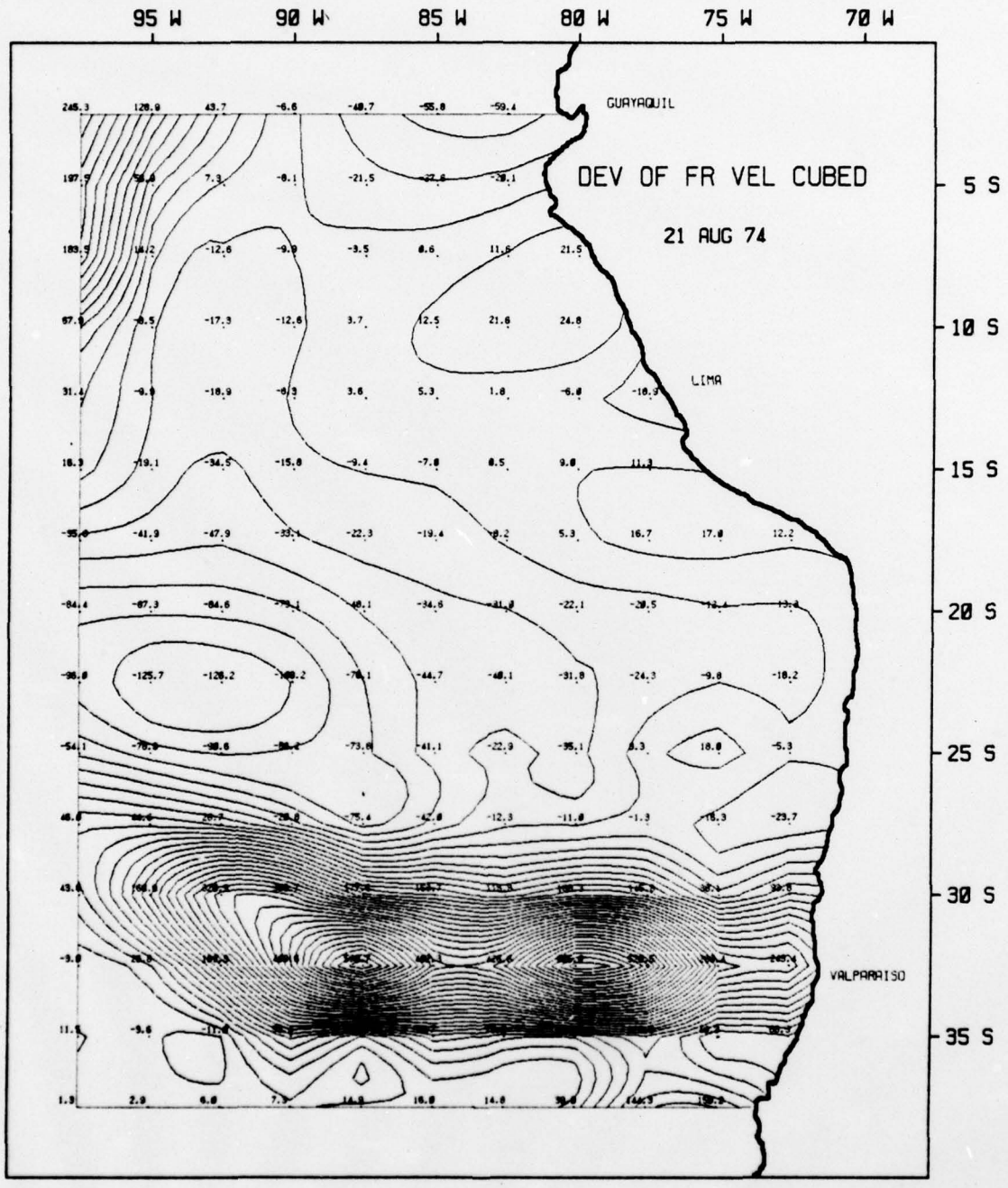

Figure 24. Deviations from the mean of U_*^3 in 10^2 cm/sec.

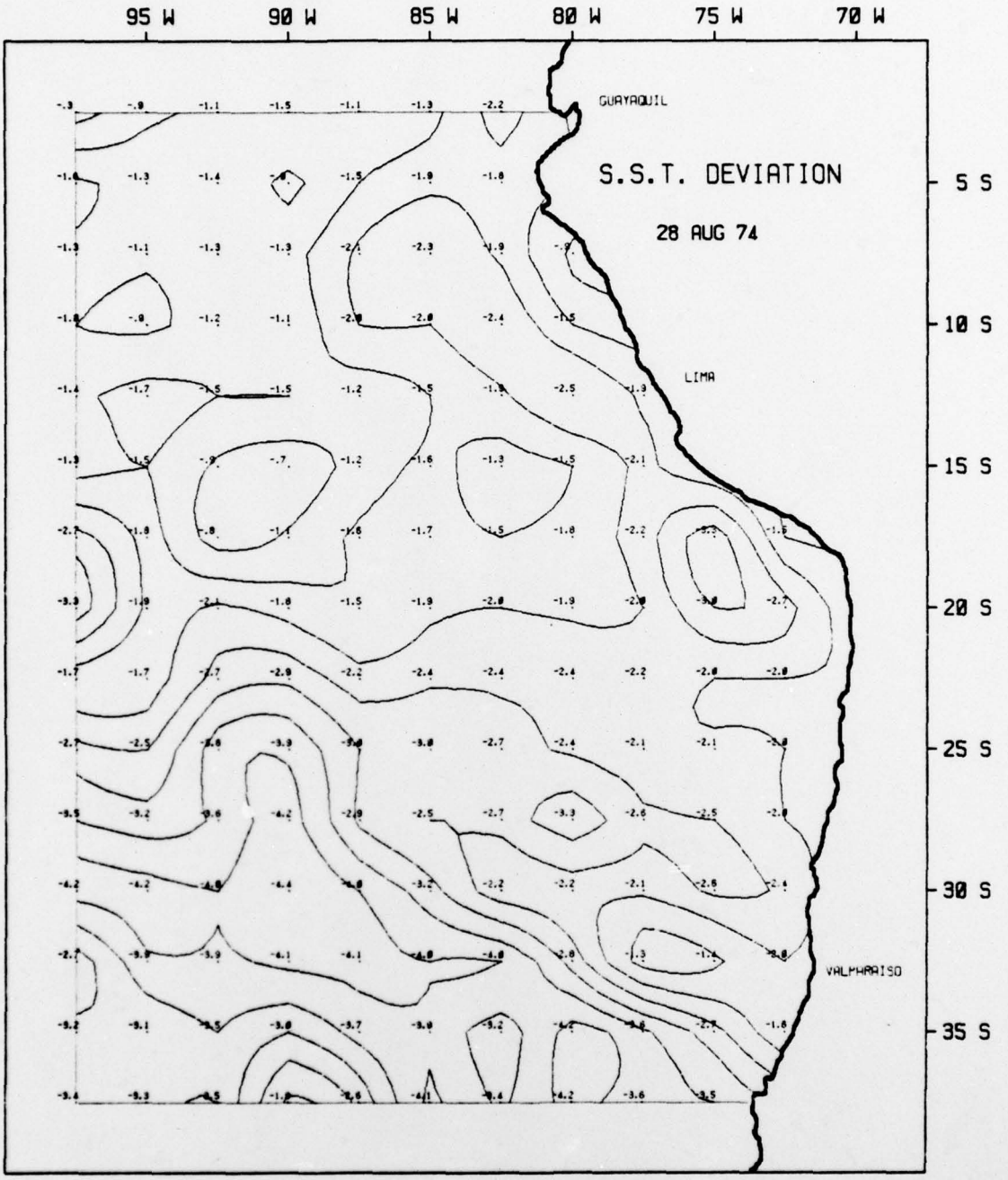

Figure 25. Sea surface temperature deviations from the mean in °C.

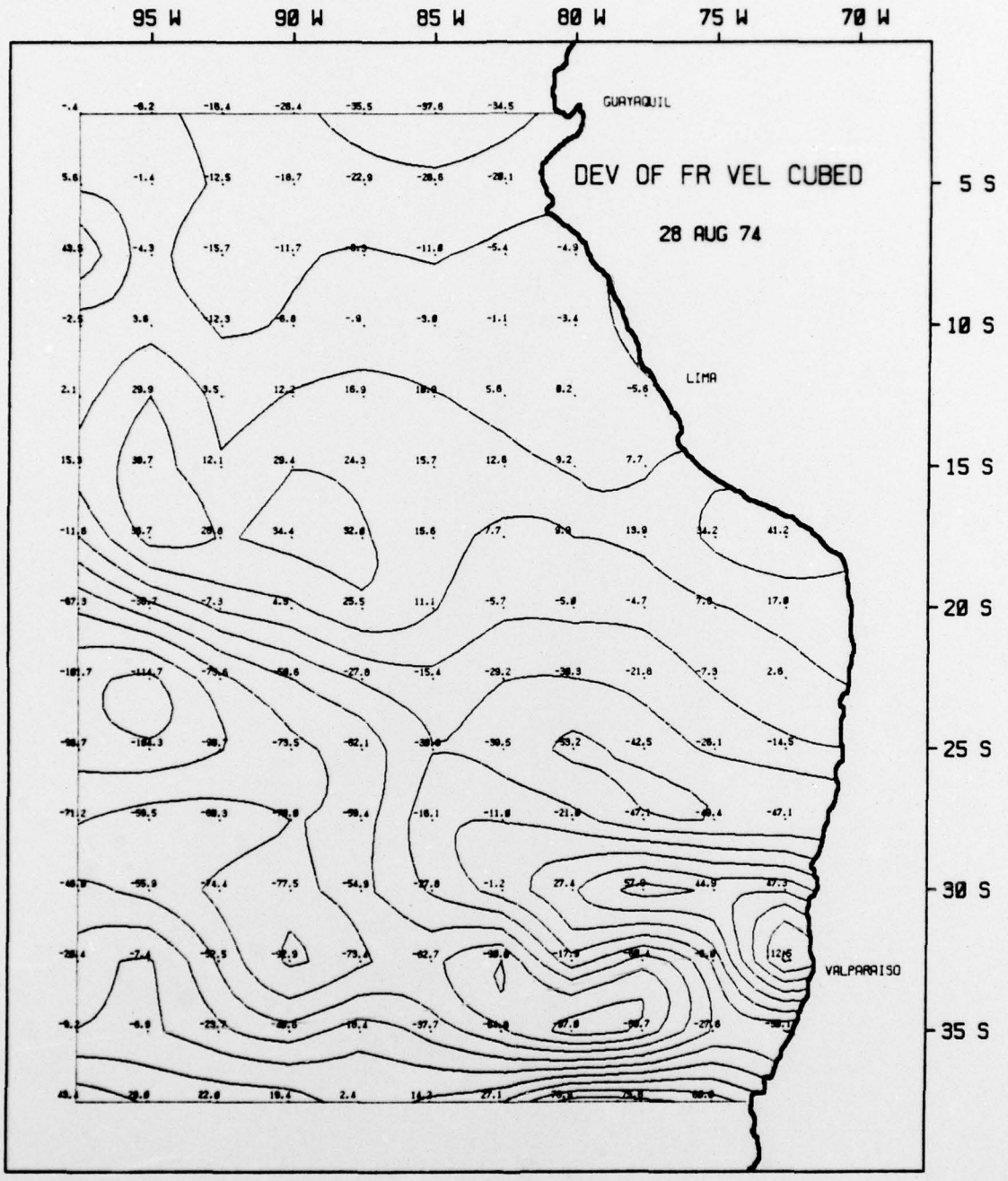

Figure 26. Deviations from the mean of U_*^3 in 10^2 cm/sec.

VI. RESULTS

To establish a statistically significant relationship between synoptic frequency fluctuations of SST', $(U_*^3)'$, and $(\text{curl}_z\ \tau)'$, some types of correlation was looked for at the five points of interest (Figure 6). The investigation points are at mid-latitudes and assumed to be unaffected by the coast. All are at 87.5° West longitude, at least 10° of longitude away from the coast.

Available for use in this study were Biomedical Computer Programs from the Health Sciences Computing Facility, University of California, Los Angeles, California, at the Computer Facility, Naval Postgraduate School. From the P-series book, the stepwise regression program BMDP2R was chosen. All standard statistical parameters were available along with regression analysis and scatter plots.

Of major interest was the normalized correlation matrix (values = 0 ± 1) which showed how well the synoptic frequency parts of $(U_*^3)'$ and $(\text{curl}_z\ \tau)'$ were related to synoptic frequency parts of SST'. Correlations r(t) were performed on these three variables with various lags of SST' with time. One lag equalled seven days. The equations used to correlate these variables were as follows:

11. $r(SST'(t + \text{lag}) \cdot (\text{curl of } \tau)'(t))$ $\quad t$ = time
12. $r(SST'(t + \text{lag}) \cdot (U_*^3)'(t))$ $\quad$ lag from 0 to $\pm$ 4 weeks

A lag of zero meant that the two variables were correlated at the same time. Lags greater than (less than) zero meant that values of SST' were compared to values of $(U_*^3)'$ and $(\text{curl}_z\ \tau)'$ in the past (future). inally, for each lag, r(t) was averaged over the year of data giving

time average lag-correlations (Table IV). A sample of the time averaged correlations at Stations #3 and #4 may be seen in Figures 27 and 28.

Each variable was also correlated with itself to see how rapidly the parameter would change with time (Table V). Graphic representation of this auto-correlation shows that the synoptic frequency oscillations in $(U_*^3)'$ and $(\text{curl}_z\ \tau)'$ occurred on a shorter time scale than that of SST' (Figure 29).

	SST' LAG / GRID #	-4	-3	-2	-1	0	+1	+2	+3	+4
(A)	1	+ .1294	+ .0806	- .0624	- .1123	- .0171	- .0506	- .0312	- .0135	+ .0909
	2	- .1519	- .2814	- .3199	- .2671	- .1564	- .0952	+ .1938	+ . 3194	+ .2877
	3	- .1774	- .1774	- .1846	- .0888	- .0152	+ .1842	+ .3513	+ .2564	+ .0543
	4	- .1323	+ .2113	+ .5295	+ .2724	+ .3706	+ .1667	- .1216	- .0884	- .3165
	5	- .0443	+ .2712	+ .2325	+ .1783	+ .1026	- .0044	+ .0489	- .2373	- .2594
(B)	1	+ .1608	- .0020	+ .0199	- .1460	- .1234	- .1343	+ .1335	+ .0411	+ .0102
	2	+ .0129	+ .1262	+ ,0705	- .0541	- .0753	- .0838	+ .0296	- .1307	- .0377
	3	+ .2542	+ .3251	+ .2854	+ .0510	+ .1206	- .0634	- .2495	- .2758	- .1132
	4	- .0055	+ .0099	+ .2564	+ .0259	+ .1845	- .0124	- .0376	+ .0198	+ .0175
	5	+ .2316	+ .0512	+ .1031	- .0085	- .1192	+ .0783	- .0691	- .0808	- .0752

Table IV. Time averaged lag correlations between SST' and $\text{curl}_z\ \tau'$(A) and $(U_*^3)'$(B) at the five selected grid points. A positive lag means SST' is evaluated at the advanced time. Each lag corresponds to seven days.

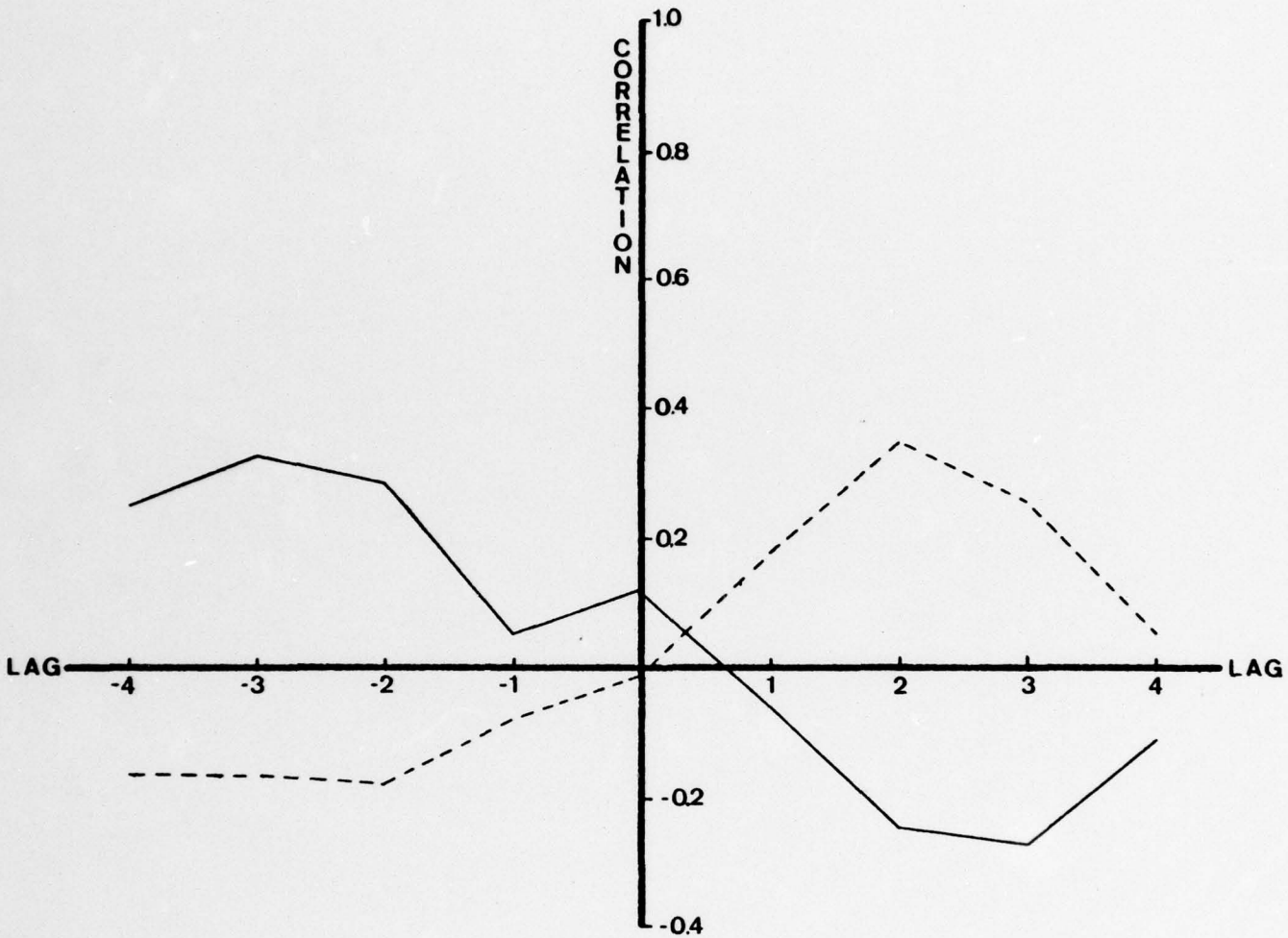

Figure 27. At Station #3 time averaged correlation of SST' with $(U_*^3)'$ as a function of lag (—) Time averaged correlation of SST' with $(\text{curl}_z\ \tau)'$ as a function of lag (---). Refer to equations 11 and 12.

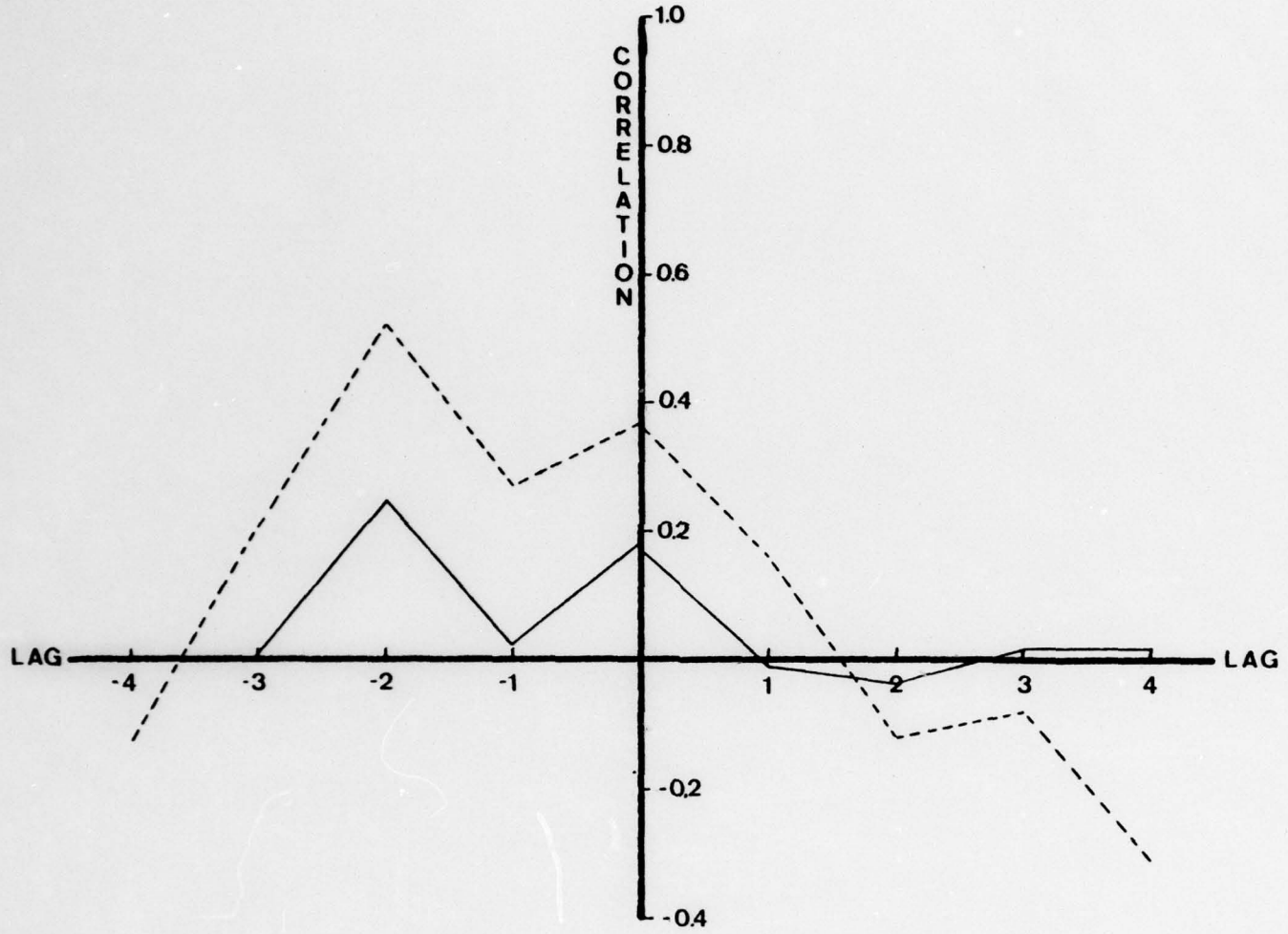

Figure 28. At Station #4 correlation of SST' with $(U_*^3)'$ as a function of lag (—) Correlation of SST' with $(\text{curl}_z\ \tau)'$ as a function of lag (---). Refer to equations 11 and 12.

STA# ↓ \ LAG →	0	±1	±2	±3	±4	
1	1.00	+ .4244	+ .0251	- .3017	- .3616	A
2	1.00	+ .5425	+ .2573	- .1191	- .3412	
3	1.00	+ .5064	+ .1412	- .1069	- .2553	
4	1.00	+ .4470	+ .1240	- .1115	- .3219	
5	1.00	+ .1062	- .1478	- .0713	- .1890	
1	1.00	- .1726	- .1584	- .2269	- .1332	B
2	1.00	+ .0116	+ .0308	- .1802	- .3101	
3	1.00	+ .1996	- .3881	- .3712	+ .1014	
4	1.00	+ .1974	- .0791	- .0791	- .2901	
5	1.00	- .0316	- .0761	+ .1739	- .3266	
1	1.00	- .0630	+ .1411	- .0847	- .2870	C
2	1.00	- .0920	- .2413	- .2225	+ .0410	
3	1.00	+ .0057	- .2400	- .1871	- .0561	
4	1.00	- .3506	- .0474	+ .0843	- .2394	
5	1.00	- .0747	- .1577	- .1860	- .1888	

Table V. Autocorrelation values for SST'(A), $curl_z\ \tau'$(B), $(U_*^3)'$(C).

VII. CONCLUSIONS

The correlation values were not what were expected. The highest correlation (+.5293) for $(\text{curl}_z\ \tau)'$ occurred at a -2 week lag of SST' at point #4, and the highest correlation (+.3251) for $(U_*^3)'$ occurred at a -3 week lag of SST' at point #3; but these results can be given little weight since they are not part of a coherent pattern in the correlation matrix.

The basic theory was that the curl of Tau when positive would produce surface Ekman convergence of ocean waters with downwelling causing warming (weak effect) of the sea surface. When the curl of Tau was negative, the surface Ekman divergence should come with upwelling and cooling (strong effect) of the sea surface. Thus the time average correlations between SST' and $(\text{curl}_z\ \tau)'$ was expected to be positive at positive lags. High surface friction wind (U_*) should cause surface mixing resulting in cooling. Thus SST' and $(U_*^3)'$ should be negatively correlated at positive lag.

In terms of having the "correct" sign of the correlations, station #3 came closest to the theoretical expectations in both the fields. If the data were perfect and could be completely trusted, it would appear that both processes, wind mixing and Ekman pumping, were occurring with approximately equal importance at the station. Qualitatively, about half the variance in non-seasonal SST fluctuations at two week periods would be properly related to these two processes. Unfortunately the results are not similar at the other locations (Table IV). In this study therefore, this basic theory was not supported by results.

The best explanation for the discrepancy between data and theory was that the Southern Hemisphere lacks a stable data base. Figure 7B, SST deviations with the seasonal cycle removed, showed SST' amplitudes ranging from 0 to $\pm$ 1.5°C. In Table I, Section V.C, where GOSSTCOMP data was compared to ship board data, the average absolute error between that of cruise data and GOSSTCOMP data was 1.17°C. Since the error was the same order of magnitude as the deviations, it was expected that these errors strongly influenced the SST deviations. There was no way in this report to verify FNWC's marine global band fields over the Pacific Ocean in the Southern Hemisphere. There were very few ocean observations in this region so there is a possibility of non-negligible errors in the surface wind fields as well. Thus, during the period of this study, the Southern Hemisphere products are of questionable accuracy.

The number of ships in the South Pacific Ocean reporting SST values, a prime source for checking satellite observations in the GOSSTCOMP routine, was definitely low compared to that of the North Pacific. It was also pertinent that there was a scarcity of weather observation platforms that fed data into FNWC from this very large region. Yet, even at present, these were the best available sources for study of the phenomena in the Eastern Pacific Ocean in the Southern Hemisphere.

The author strongly recommends that further investigation into this area be encouraged. More research in the Eastern South Pacific would provide a broader study base to facilitate a better understanding of the changes in this region's ocean temperatures.

LIST OF REFERENCES

BIOMEDICAL COMPUTER PROGRAMS
1975. BMDP2R - Stepwise Regression, Health Sciences Computing Facility, Program revised Feb. 76, W. J. Dixon, ed., University of California Press, Los Angeles.

BROWER, R. L., GOHRBAND, H. S., PICHEL, W. G., SIGNORE, T. L., WALTON, C. C., 1976. Satellite Derived Sea Surface Temperatures from NOAA Spacecraft, NOAA/NESS Technical Memorandum #78, Washington, D. C.

EL NINO WATCH--UNDERWAY PROGRAM
1976. Thermosalinograph Data and XBT Log, 11 Feb 1975, to 27 May 1975, Data report prepared by GEOSECS Operations Group/NSF, A. E. Bainbridge, Project Director, R/V MONAWAVE, University of Hawaii.

FISHING INFORMATION
May 1974 #5; June 1974 #6; July 1974 #7; August 1974 #8; September 1974 #9; October 1974 #10; November 1974 #11, December 1974 #12; January 1975 #1; February 1975 #2; March 1975 #3; April 1974 #4; May 1975 #5; U. S. Department of Commerce, NOAA, National Marine Fisheries Service, Southwest Fisheries Center, La Jolla, California.

GLOSSARY OF METEOROLOGY
1959. R. E. Huschke, ed., American Meteorological Society, Boston, Mass.

HANTEL, M.
1970. Monthly charts of surface wind stress curl over the Indian Ocean, Monthly Weather Review, V 98.

NELSON, C. S.
1976. Wind stress and wind stress curl over the California Current, M.S. Thesis in Oceanography, Naval Postgraduate School, Monterey, California.

WYRTKI, K., STROUP, E., PATZERT, W., WILLIAMS, R., QUINN W.
1976. Predicting and Observing El Nino, Science, V 191, #4225.

INITIAL DISTRIBUTION LIST

		No. Copies
1.	Department of Oceanography, Code 68 Naval Postgraduate School Monterey, California 93940	3
2.	Oceanographer of the Navy Hoffman Building No. 2 200 Stovall Street Alexandria, Virginia 22332	1
3.	Office of Naval Research Code 410 NORDA, NSTL Bay St. Louis, Mississippi 39520	1
4.	Dr. Robert E. Stevenson Scientific Liaison Office, ONR Scripps Institution of Oceanography La Jolla, California 92037	1
5.	Library, Code 3330 Naval Oceanographic Office Washington, D. C. 20373	1
6.	SIO Library University of California, San Diego P. O. Box 2367 La Jolla, California 92037	1
7.	Department of Oceanography Library University of Washington Seattle, Washington 98105	1
8.	Department of Oceanography Library Oregon State University Corvallis, Oregon 97331	1
9.	Commanding Officer Fleet Numerical Weather Central Monterey, California 93940	1
10.	Commanding Officer Naval Environmental Prediction Research Facility Monterey, California 93940	1

11.	Department of the Navy Commander Oceanographic System Pacific Box 1390 FPO San Francisco 96610	1
12.	Defense Documentation Center Cameron Station Alexandria, Virginia 22314	2
13.	Library (Code 0142) Naval Postgraduate School Monterey, California 93940	2
14.	Director Naval Oceanography and Meteorology National Space Technology Laboratories Bay St. Louis, Mississippi 39520	1
15.	NORDA Bay St. Louis, Mississippi 39520	1
16.	Prof. R. L. Haney, Code 63Hy Department of Meteorology Naval Postgraduate School Monterey, California 93940	2
17.	Prof. G. J. Haltiner, Chairman Department of Meteorology Naval Postgraduate School Monterey, California 93940	1
18.	Meteorology Department Code 63 Library Naval Postgraduate School Monterey, California 93940	1
19.	Defense Mapping Agency Inter-American Geodetic Survey Drawer 934 Fort Clayton, Canal Zone	4
20.	Assoc. Prof. J. B. Wickham, Code 68Wk Department of Oceanography Naval Postgraduate School Monterey, California 93940	2
21.	Prof. Klaus Wyrtki Department of Oceanography University of Hawaii Honolulu, Hawaii 96822	1
22.	Dr. Robert L. Bernstein Scripps Institution of Oceanography La Jolla, California 92037	1

23. Lt. George H. Berry
100 Brownell Circle
Monterey, California 93940 1

24. Lt. Craig S. Nelson
Pacific Environmental Group
National Marine Fisheries Service
c/o Fleet Numerical Weather Central
Monterey, California 93940 1

25. Dr. Alan E. Strong, Oceanographer
Environmental Sciences Group
U. S. Department of Commerce
National Oceanic and Atmospheric Administration
National Environmental Satellite Service
Washington, D. C. 20233 1

26. Dr. Paul McClain
Environmental Sciences Group
U. S. Department of Commerce
National Oceanic and Atmospheric Administration
National Environmental Satellite Service
Washington, D. C. 20233 1

27. Defense Mapping Agency
Hydrographic Center
Technical Library, Code LAL
Washington, D. C. 20390 1